Communications in Transportation Research 5 (2025) 100230

Contents lists available at ScienceDirect

Communications in Transportation Research

journal homepage: www.journals.elsevier.com/communications-in-transportation-research

Full Length Article

Quantitative assessment of mid-air collision probability in urban air mobility: A safety barrier-based framework for integrated operations

Jinpeng Zhang[a], Yan Xu[a,*], Kaiquan Cai[a], Victor Gordo[b], Gokhan Inalhan[c]

[a] School of Electronic Information Engineering, Beihang University, Beijing, 100191, China
[b] Ingeniería y Economía del Transporte (INECO), Madrid, 28036, Spain
[c] Sloane Institute, London, W1W5PF, UK

ARTICLE INFO

Keywords:
urban air mobility (UAM)
mid-air collision (MAC)
risk assessment
integrated operations
safety barriers

ABSTRACT

Risk assessment is a key issue when handling the increasing use of unmanned aircraft systems (UASs), especially in integrated operational urban airspace. This study proposes a method to systematically quantify the mid-air collision (MAC) risk for different operation types in urban air mobility (UAM). Specifically, a novel assessment framework is formulated that includes three timelines to track risk evolution for integrated operations (i.e., cooperative, non-cooperative, and manned aircraft) and four safety barriers (i.e., procedural, strategic, tactical, and collision avoidance mitigation) to prevent a conflict ending in MAC. Under the framework, analytical models are established considering trajectory uncertainty, latency time, and detection and avoidance (DAA) system risk ratio to calculate the failure probability of each barrier, and thus an overall MAC probability. Result-oriented, process-oriented and comprehensive Monte Carlo simulations are constructed to validate the proposed models and the MAC assessment timeline, followed by demonstrating four operational scenarios in real-world environment to illustrate the assessment process of the method. Results show that the simulation probability curves closely match the theoretical predictions. The cooperative UAS contributes the highest MAC risk in our designed integrated environment, with strategic mitigation failures accounting for the largest proportion, and thus effective strategic trajectory planning is crucial for maintaining the safety of integrated operations.

1. Introduction

Urban low-altitude airspace is a valuable natural resource with significant socio-economic importance, and the rational management of urban airspace is crucial for alleviating traffic congestion and reducing the incidence of ground traffic accidents. Recently, unmanned aircraft systems (UASs) have been widely used in urban low-altitude airspace for various tasks, such as logistics and transportation, aerial photography and mapping, and emergency rescue (Garrow et al., 2021; Saeed et al., 2021). The majority of UAS engaged in these activities operate separately from manned aircraft in current airspace. As their numbers continue to rise, the limited airspace will face growing inefficiencies and increased risk due to the insufficient capacity. As a result, solutions for UAS operation in controlled airspace, particularly the concept of integrated operations between manned aircraft and UAS, are gaining significant attention. The European Union released the "Drone Strategy 2.0" to promote the integration of UAS, the strategy advocates considering air traffic management (ATM) and U-space together so that, by the time the full U-space is deployed, the two environments will have become one, fully integrated airspace (Scott and Andritsos, 2023). Within the framework of the SESAR program, the AURA project (ATM U-space Interface) explores the concepts and technologies needed for safe and seamless interaction between current ATM systems and U-space operations, with the aim of managing high volumes of manned and unmanned traffic operating safely and concurrently in shared airspace. Building on this, the ENSURE project is refining a common interface and services for U-space and ATM, developing a standardized data model and a dynamic airspace configuration service to ensure safe separation between manned and unmanned aircraft (Teutsch, 2023). Similarly, the SESAR JU project GOF 2.0 Integrated Urban Airspace is demonstrating how UAS and air taxis can safely, securely, and sustainably share urban airspace (Schwoch et al., 2024). Following this trend, the urban airspace system is gradually evolving from manned aviation through hybrid operations with UAS to eventually integrated operations.

The integrated operation increases the density and complexity of the airspace, exposing aircraft to multiple sources of collision risks,

* Corresponding author.
E-mail address: yan.xu@buaa.edu.cn (Y. Xu).

https://doi.org/10.1016/j.commtr.2025.100230
Received 4 July 2025; Received in revised form 10 September 2025; Accepted 11 September 2025
Available online 5 December 2025
2772-4247/© 2025 The Authors. Published by Elsevier Ltd on behalf of Tsinghua University Press. This is an open access article under the CC BY-NC-ND license (http://creativecommons.org/licenses/by-nc-nd/4.0/).

including cooperative UAS, non-cooperative UAS, and manned aircraft. These risks pose significant hazards not only to other aircraft but also to people and infrastructure on the ground, making operational safety a critical challenge for urban air mobility (UAM). The primary obstacle lies in accurately assessing mid-air collision (MAC) risks, which is a prerequisite for conflict resolution techniques and a key component of urban air traffic management.

In the literature, operation risk assessment between UAS and other UAS or between UAS and manned aircraft has been extensively studied. Some scholars further divide UAS into cooperative UAS and non-cooperative UAS. The flight information of cooperative UAS is publicly available or the supervisory authorities can query or record their flight trajectories. In contrast, the information of non-cooperative UAS can only be detected directly by some sensors like radar and their flight intentions cannot be perceived, so there are different MAC assessment methods for these two types of UAS.

For cooperative UAS, existing approaches can be divided into two categories: geometric conflict methods and probabilistic calculation methods. The former establishes geometric analysis models based on the relationship between positions and velocities of UAS pairs to determine the potential MAC risks. A representative example is the speed obstacle model. Choi et al. (2017) used the speed obstacle method to detect environmental information when the perception ability of UAS is limited, enabling the selection of collision-free trajectories. Velasco et al. (2015) improved the classical speed obstacle theory based on intention information and proposed an analytical mathematical form to detect the risk of conflict quickly. However, these methods primarily rely on geometric relationships to qualitatively determine potential conflicts between UAS pairs, lacking a robust quantitative assessment of conflict risk. Additionally, since aircraft trajectories may not strictly follow their current velocity directions, such methods may exhibit accuracy limitations in risk assessment over a long time span.

More and more scholars have proposed probabilistic calculation methods to ensure the convincing of assessment results, including analytical solution derivation and sampling analysis. Paielli and Erzberger (1997) modeled the aircraft's error envelope in two-dimensional space using an elliptical shape and proposed a mathematical analysis method to estimate the conflict probability efficiently for aircraft pairs in free flight. Zou et al. (2021) decoupled the multi-dimensional integrals of various collision envelopes through integral linear and nonlinear transformations, thereby simplifying the computation of collision probability. Zhong et al. (2024) developed a UAS risk assessment model by defining position probability density functions using total system error (TSE) limits. Liu and Hwang (2011) established a trajectory prediction model with reference to Markov process and approximated the collision probability through Gaussian error. However, the above methods are limited to two UAS and cannot assess the superimposed risk posed by multiple UAS, thus failing to meet the needs of high-density operations in UAM. Zhang et al. (2022) combined the characteristics of deterministic and probabilistic methods to solve the real-time and accuracy problems in large-scale UAS conflict detection. Xiang et al. (2016) measured the safety level between multiple UAS based on the position uncertainty characterized by Brownian motion.

For non-cooperative UAS, two primary models have been extensively researched over several decades: the Monte Carlo simulation model and the gas model. Wang et al. (2018, 2019) focused on the worst-case scenario where non-cooperative intruders maintain direct collision trajectories, integrating Monte Carlo simulation and ground-assisted correction mechanisms to enhance the reliability of path prediction. However, the speed directions of non-cooperative UAS in real situations are uncertain, so the above assumptions bias the estimated MAC probability. Another widely used model for MAC assessment with non-cooperative UAS is the gas model, in which UASs are assumed to move with random intent and unpredictable trajectories, similar to free-moving gas molecules. Based on the assumption of this uncertain behavior, Su and Xu (2024) measured the probability of an aircraft being invaded by non-cooperative UAS within a fixed mission time. The gas model offers distinct advantages in MAC risk quantification, particularly in its ability to assess uniformly distributed risks throughout mission execution without requiring specific information about other aircraft's positions or flight intentions.

For manned aircraft, the Monte Carlo simulation is still the dominant method. Pothana et al. (2023) fitted the velocity, heading, and altitude of UAS using a Gaussian distribution and determined the MAC risk near the airport by comparing the possible position of UAS with the historical ADS-B data from manned aircraft. Wang et al. (2020) constructed a 3-D Monte Carlo positional distribution model based on the flight dynamics of UAS, so as to establish the alert zone boundaries around the airport. In addition, geometric conflict methods are also used to assess the risk of manned aircraft. la Cour-Harbo and Schiøler (2019) established a geometric encounter model based on physical parameters of manned aircraft and operational statistics of general aviation traffic to generate the conflict probability for flights below 500 feet. Complementary research efforts have focused on modeling airport terminal area structures to analyze manned aircraft flight patterns and evaluate collision risks (Hu et al., 2020; McFadyen et al., 2018).

The above methods characterize the MAC probability for cooperative UAS, non-cooperative UAS or manned aircraft from different perspectives such as analytical solution, sampling analysis and geometric relations, but the common drawback is that they treat the risk as a process of continuous deterioration and do not take into account mitigation measures in actual operations. The specific operations risk assessment (SORA) approach published by the Joint Authorities for Rulemaking of Unmanned Systems (JARUS) (2024) provides clear guidelines for assessing operational risks, which identify the sources and consequences that lead to both air and ground risks. Some scholars have conducted research on low-altitude operations based on SORA, such as determining separation minima (Zou et al., 2021) and designing flight procedures (Miles et al., 2019). However, SORA is a qualitative method that only classifies the collision risk from manned aircraft based on the proximity to aerodromes and controlled airspace volumes, while lacking a specific metric for quantifying the level of safety. Recently, Vila Carbó et al. (2023) proposed a probabilistic methodology for performing quantitative risk assessment considering the strategic and tactical mitigation. However, this method is limited to non-cooperative UAS and does not consider other risk sources or corresponding mitigation measures in the integrated operations, thus requiring further improvement.

The following research gaps have been identified, including: (1) Integrated operations face multi-source MAC risks, yet current studies lack a comprehensive framework and standardized methodology for assessing these heterogeneous risk factors, rendering them inadequate for application in integrated airspace. (2) Most existing studies focus on directly computing final risk outcomes, neglecting a systematic analysis of the complete MAC evolution process. (3) Current studies have not adequately considered critical environmental factors such as wind effects, information latencies, total system error, and airborne sensor inaccuracies, and have paid limited attention to the potential impact of multiple avoidance maneuvers enabled by advanced aircraft performance. (4) The prevailing Monte Carlo methods are typically used for risk assessment rather than model validation, leading to high computational costs and slow convergence rates, which makes them ineffective for real-time risk assessment, particularly during in-flight operations.

To address the research gaps mentioned above, we systematically analyze the evolution of MAC risk for different operation types, and explore the multi-level safety barriers and their failure causes throughout the process, so as to form a comprehensive risk assessment methodology. Table 1 provides a summary of the most related surveys in the field of MAC risk assessment, which shows that this research is the first study that integrates multi-type operations and safety barriers into the MAC assessment and considers various errors such as sensors and wind. The main contributions of this study are summarized as follows:

Table 1
Related works comparison.

Ref.	Object	Multiple object	Mitigation measure	Error	Method	Result
Choi et al. (2017)	Cooperative	—	—	—	Speed obstacle	Qualitative
Velasco et al. (2015)	Cooperative	—	—	—	Speed obstacle	Qualitative
Paielli and Erzberger (1997)	Cooperative	—	—	FTE; FSE	Mathematical derivation	Quantitative
Zou et al. (2021)	Cooperative	—	—	FTE; FSE	Mathematical derivation	Quantitative
Zhong et al. (2024)	Cooperative	—	—	FTE; wind	Mathematical derivation	Quantitative
Liu and Hwang (2011)	Cooperative	—	—	Heading	Integral solution	Quantitative
Zhang et al. (2022)	Cooperative	✓	—	FTE; FSE	Integral solution	Quantitative
Xiang et al. (2016)	Cooperative	✓	—	FTE	Mathematical derivation	Quantitative
Wang et al. (2018)	Non-cooperative	✓	—	Thrust	Monte Carlo	Quantitative
Su and Xu (2024)	Non-cooperative	✓	Strategic; tactical	sensor; wind	Gas model	Quantitative
Pothana et al. (2023)	Manned aircraft	✓	—	Speed; heading	Monte Carlo	Quantitative
Wang et al. (2020)	Manned aircraft	—	—	Drag; trust	Monte Carlo model	Quantitative
la Cour-Harbo and Schiøler (2019)	Manned aircraft	✓	—	—	Integral solution	Quantitative
Vila Carbó et al. (2023)	Cooperative	—	Strategic; tactical	FTE; FSE	Reich model; Mathematical derivation	Quantitative
This study	Cooperative Non-cooperative Manned aircraft	✓	Procedure; strategic; tactical; avoidance	FTE; FSE; sensor error; wind	Gas model; Mathematical derivation	Quantitative

- A comprehensive MAC probability assessment framework applicable to multi-type operations is proposed, including cooperative UAS, non-cooperative UAS, and manned aircraft, which enhances the SORA method by extending its air risk scope beyond the conventional manned aircraft.
- Three MAC evolution timelines designated to multi-type operations are formulated, covering four main safety barriers for preventing a conflict ending in a MAC. This leads to a careful MAC probability prediction considering all barriers have failed, which delves the SORA method by providing quantitative justifications.
- For strategic mitigation, errors due to various external factors are incorporated into an analytical solution of conflict probability to quickly determine whether a UAS poses a threat in three-dimensional space. For tactical mitigation, multiple maneuver strategies and a latency time determination function are established to further improve the accuracy of the results.
- Result-oriented, process-oriented and comprehensive Monte Carlo simulations, designed to meet different validation objectives, are combined with various external factors (i.e., total system error, latencies and sensor errors) to validate the accuracy of the proposed models. Furthermore, a real-world environment including four typical scenarios (i.e., three types of operation individually and their integrated operations collectively) is established to illustrate the application of this method.

The paper is organized as follows: in Section 2, the MAC probability assessment framework is presented, which is the foundation of this assessment method; Section 3 presents the specific models including the risk envelope model and the mitigation failure models for four barriers, so as to characterize the failure probability at each stage, and then the MAC probability; Section 4 sets the simulation scenarios and performs Monte Carlo simulation to validate the accuracy of the proposed models; Section 5 illustrates a real-world case study to present the assessment results of this method. In the Appendix, the interlayer interactions are incorporated into the assessment framework to further capture the dependencies between adjacent mitigation measures. In the Appendix, interlayer interactions are incorporated into the assessment framework to explore the dependencies between adjacent barriers.

2. Framework

To address MAC risk assessment requirements of specific aircraft in integrated airspace, a comprehensive assessment framework containing three timelines is developed to describe the MAC evolution of various operation types, as shown in Fig. 1. In this framework, the aircraft under assessment is referred to as the ownship and is modeled as an eVTOL, which is representative of future integrated airspace and capable of both manned and unmanned flight. The ownship primarily faces MAC risks from three operation types: cooperative UAS, non-cooperative UAS, and manned aircraft. The first two refer to small drones, while the latter denotes civil airliners, which are collectively referred to as intruders in this paper.

Referring to the swiss-cheese model (SWM) (Chandler and Giesecke, 1983), this framework views MAC as the detrimental result of the simultaneous failure of multiple safety barriers, further categorized into the failure of procedural mitigation, strategic mitigation, tactical mitigation, and collision avoidance. In the widely adopted SWM theory, failures at different defense layers are treated as mutually independent events (International Civil Aviation Organization (ICAO), 2018; Reason et al., 2006). Existing studies (Xue and Fu, 2018) have applied the SWM to aviation accident analysis, suggesting that accidents often result from multiple independent deficiencies. Following this assumption, the framework likewise treats the mitigation measures in safety barriers as independent and explores the interaction among them in the Appendix.

Procedural mitigation measures are developed during the airspace planning phase, mainly through mandatory measures such as airspace isolation or operational limits to prohibit the entry of UAS into essential areas. In integrated airspace, operational safety for ownship is typically ensured through the implementation and management of dynamic corridors. However, the untimely opening of these corridors may lead to intrusions by either non-cooperative or manned aircraft, thereby compromising the protective efficacy of the corridor system, which is the main reason why procedural mitigation measures fail.

Strategic mitigation measures are developed before the cooperative UAS flight, primarily through flight authorization to prevent temporal and spatial overlaps among cooperative UAS, such as the non-conflicting four-dimensional trajectory planning based on the corridors. The main failure reasons are operational uncertainties during flight, such as wind impact, navigation error, and flight technical error, which may cause trajectory deviation, and then the situation of tactical conflict.

Tactical mitigation measures refer to the tactical separation resolution provided by actors such as UTM service supplier (USS) or U-space service provider (USSP). When receiving the warning of strategic mitigation failure, they can issue maneuver advisories or instructions to the

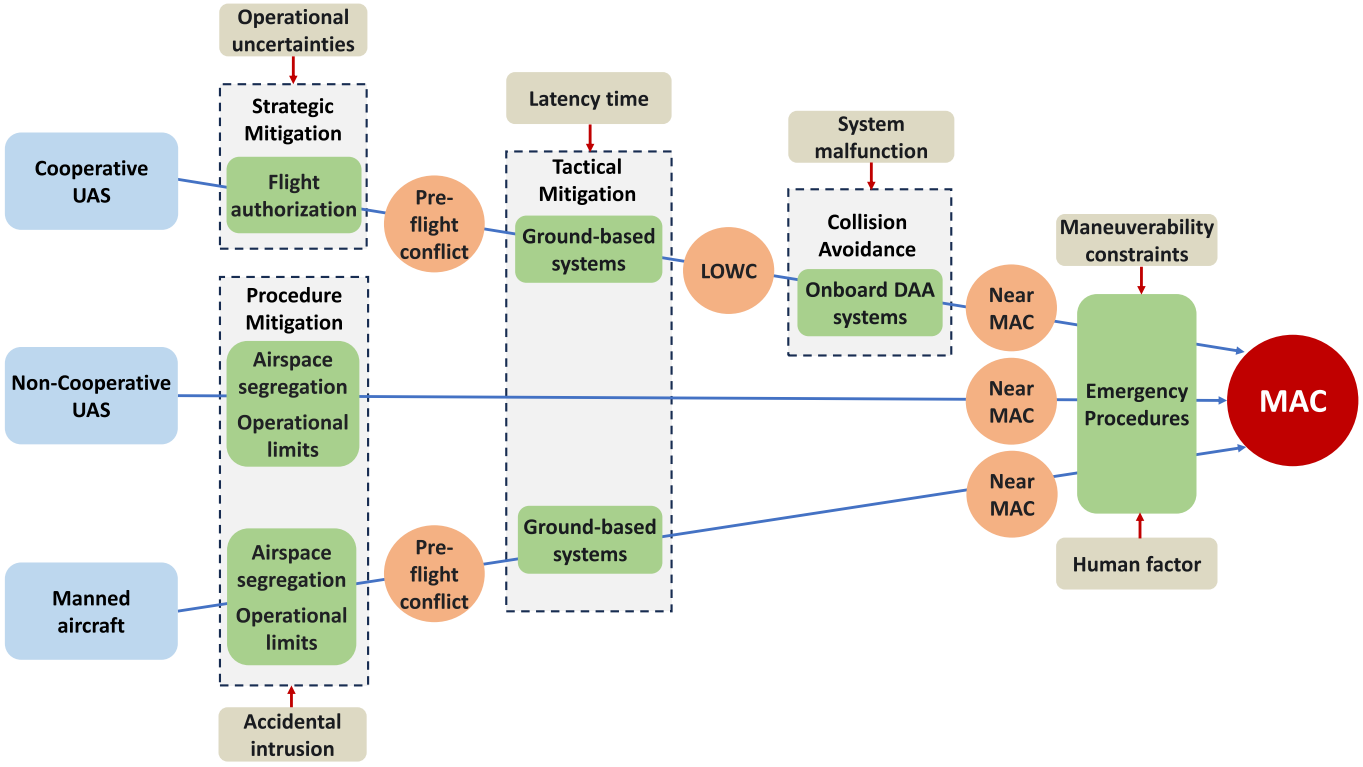


Fig. 1. Overall framework diagram for MAC probability assessment.

aircraft to avoid the loss of well-clear (LOWC) situation. However, executing maneuvers requires response time (i.e., latency time) due to some reasons such as pilot reaction and communication transmission. If the aircraft's predicted approach time to the DAA well-clear (DWC) volume is less than that time (i.e., the aircraft enters the DWC before it has time to complete the maneuver), tactical mitigation failure will occur.

Collision avoidance is the next mitigation barrier during flight, mainly for the measures provided by the onboard DAA system, which is initiated immediately by the onboard flight computer when tactical mitigation measures have failed. Due to the close distance between an aircraft pair at that moment and the endogenous malfunction probability of the DAA system, this measure also has the possibility of failure.

After collision avoidance failure, the two aircraft involved have reached the state of near mid-air collision (NMAC), the probability of such a NMAC developing into an actual collision at this point is subject to providence (P_{pro}). As the inability to accurately simulate "providence", we assume a worst-case scenario where a collision must occur if the collision avoidance fails, i.e., $P_{\text{pro}} = 1$ in such a case.

Based on the above framework, the MAC probability assessment

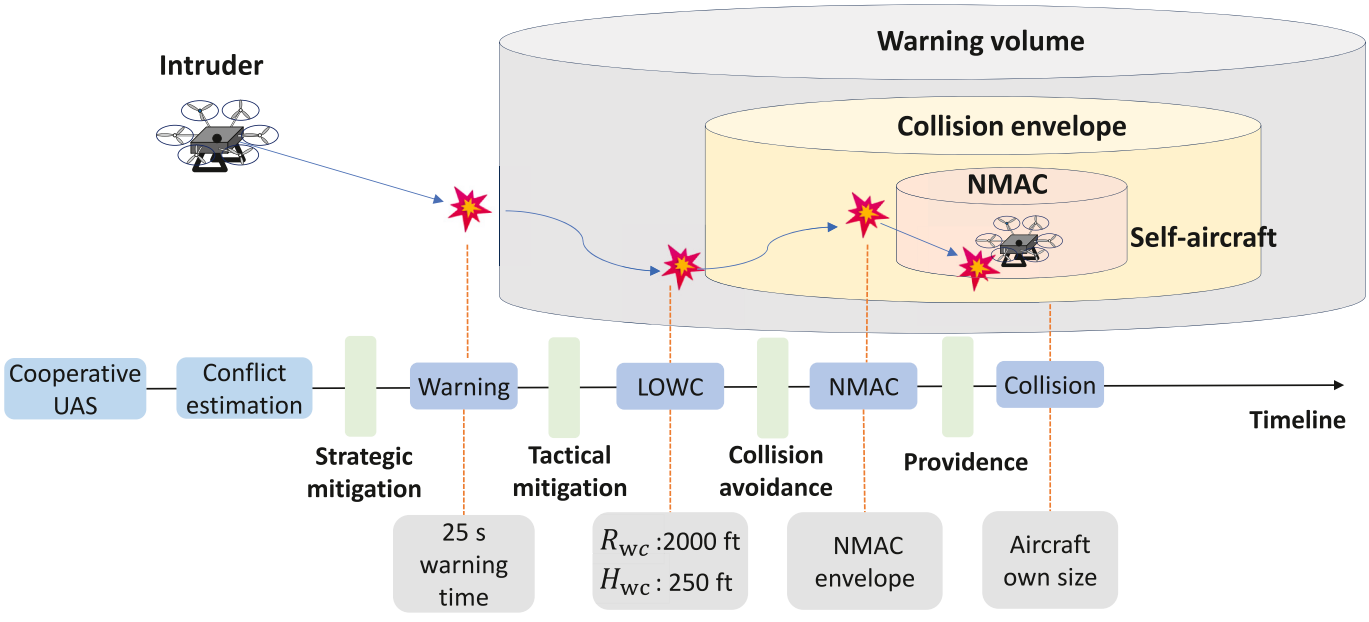


Fig. 2. Timeline of the process from intruder encounter to MAC for the ownship.

processes and timelines for different operation types are designed separately.

2.1. MAC evolution timeline for cooperative UAS

The origin of MAC risk between cooperative UAS is mainly a strategic conflict caused by operational uncertainty, which evolves into a series of subsequent risk events. To assess the MAC probability of cooperative UAS systematically, we formulate an encounter timeline, as shown in Fig. 2, to connect the events that lead to the occurrence of MAC and identify the failure signs for each barrier, which consist of three phases:

Phase 1: A conflict probability estimation model during the encounter is proposed to characterize the probability of spatiotemporal overlap of UAS pairs due to operational uncertainty, that is, the probability of strategic mitigation failure expressed by $P_{\mathrm{ST}}^{\mathrm{cop}}$. The encounter period is a key parameter in the model, we introduce a warning mechanism according to the detect and avoid alerting logic (DAIDALUS) (Muñoz et al., 2015), which requires that the warning will be issued if intruders with constant velocities enter the DWC volume within 25 s. Consequently, we define the encounter period as 25 s and calculate the conflict probability between two UAS within this time scale.

Phase 2: After strategic mitigation fails, the ownship performs maneuvers according to the relevant instructions to prevent the intruder from entering the collision envelope. Based on the DWC envelope introduced in Cone et al. (2019), this paper defines the concept of collision envelope as a cylinder that encompasses the DWC volume and the uncertainty area, which will be described in Section 3.1. A maximum approach time estimation model is established to estimate the time allowed to fly after receiving the strategic failure warning, and the probability of tactical mitigation failure after strategic mitigation $P_{\mathrm{TC-ST}}^{\mathrm{cop}}$ is determined by comparing it against the latency time.

Phase 3: The collision avoidance measures dominated by the airborne DAA system control the aircraft to avoid obstacles automatically, and we summarize the endogenous failure rate by analyzing the historical data as the collision avoidance failure probability after tactical mitigation $P_{\mathrm{CA-TC}}^{\mathrm{cop}}$. If this measure fails, the two aircraft enter the NMAC and the MAC between them depends on providence.

Therefore, the MAC probability for ownship with respect to cooperative UAS i is

$$P_{\mathrm{cop}-i} = P_{\mathrm{ST}}^{\mathrm{cop}-i} \cdot P_{\mathrm{TC-ST}}^{\mathrm{cop}-i} \cdot P_{\mathrm{CA-TC}}^{\mathrm{cop}-i} \cdot P_{\mathrm{pro}-i} \tag{1}$$

Since the flight plan of cooperative UAS is known, the MAC risk associated with each individual UAS can be independently assessed, enabling the determination of MAC risk (P_{cop}) posed by all cooperative UAS within the airspace:

$$P_{\mathrm{cop}} = 1 - \prod_{i=0}^{n} \left(1 - P_{\mathrm{cop}-i}\right) \tag{2}$$

2.2. MAC evolution timeline for non-cooperative UAS

Due to the unpredictability of non-cooperative UAS's movement trends, targeted mitigation is unfeasible after intrusion. The MAC evolution timeline for non-cooperative UAS involves only procedural mitigation strategies, i.e., airspace isolation measures. Furthermore, given the inability to precisely obtain the number of non-cooperative UAS intrusions, we establish a dynamic GAS model to quantify the probability of non-cooperative UAS intrusion $P_{\mathrm{PC}}^{\mathrm{non\text{-}cop}}$ during mission execution from a global perspective. A MAC is considered to have occurred if this procedural mitigation measure fails, as shown in Eq. (3):

$$P_{\mathrm{non\text{-}cop}} = P_{\mathrm{PC}}^{\mathrm{non\text{-}cop}} \cdot P_{\mathrm{pro}} \tag{3}$$

2.3. MAC evolution timeline for manned aircraft

Manned aircraft are susceptible to UAS during the take-off and landing phases, so the first barrier to preventing MAC between UAS and manned aircraft is procedural mitigation measures, specifically through dynamic corridor management in integrated airspace to ensure temporal and spatial separation near terminal areas. We establish a GAS model based on the STAR and SID routes to characterize the probability of procedural mitigation failure $P_{\mathrm{PC}}^{\mathrm{man}}$. If a UAS intrudes into the STAR and SID area during manned aircraft operations, the UAS will receive maneuver instructions (from USSP directly or ATC via USSP). This process can be summarized as tactical conflict mitigation after procedural mitigation, and the failure probability $P_{\mathrm{TC-PC}}^{\mathrm{man}}$ can be estimated using the maximum approach time estimation model, so the MAC probability with manned aircraft is

$$P_{\mathrm{man}} = P_{\mathrm{PC}}^{\mathrm{man}} \cdot P_{\mathrm{TC-PC}}^{\mathrm{man}} \cdot P_{\mathrm{pro}} \tag{4}$$

From the perspective of the ownship, it is necessary to assess the MAC probability caused by all intruders in the airspace, i.e., the overall MAC probability. This paper introduces a metric, namely "collision probability per flight time", to quantify the result of the assessment, which can be expressed as the superposition of the maximum risk value posed by the three types of intruder during a fixed flight time, as shown in Eq. (5). It is crucial to highlight that the MAC probability for non-cooperative UAS and manned aircraft within the airspace is directly derived from the GAS model, eliminating the need to assess the risk posed by each individual aircraft separately, as is required for cooperative UAS.

$$P_{\mathrm{all}} = 1 - \left(1 - P_{\mathrm{cop}}\right) \cdot \left(1 - P_{\mathrm{non\text{-}cop}}\right) \cdot \left(1 - P_{\mathrm{man}}\right) \tag{5}$$

where P_{cop}, $P_{\mathrm{non\text{-}cop}}$, and P_{man} represent the maximum MAC probability with cooperative UAS, non-cooperative UAS, and manned aircraft in a time period, respectively.

The models used in the MAC probability assessment are shown in Table 2, and the modeling process and characteristics of each model will be presented subsequently.

3. Methodology

The MAC probability P_{cop}, $P_{\mathrm{non\text{-}cop}}$, and P_{man} is modeled in detail, and each part is represented with the analytical solution around Eq. (5).

3.1. UAS collision envelope

The collision envelope is defined as a cylindrical volume, similar in

Table 2
Summary of the models applied to the MAC probability assessment method.

	Procedural mitigation	Strategic mitigation	Strategic mitigation	Strategic mitigation
Cooperative UAS	—	The conflict probability estimation model during encounter	The maximum approach time estimation model	The risk ratio of DAA systems
Non-cooperative UAS	The dynamic gas model	—	—	—
Manned aircraft	The dynamic gas model	—	The maximum approach time estimation model	—

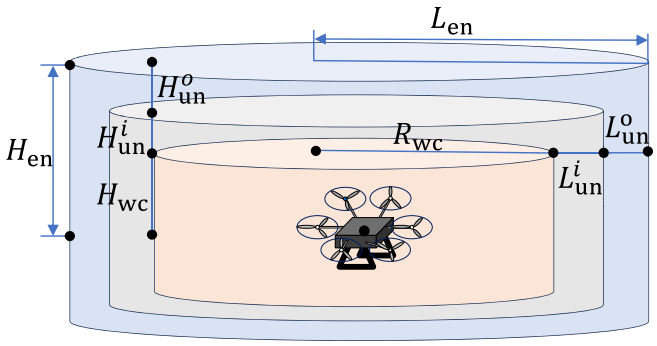


Fig. 3. Collision envelope including DWC volume and in-flight uncertainty.

form to the DWC volume, and its scope includes both the DWC area and an additional uncertainty area, as illustrated in Fig. 3. An NMAC is considered to occur when an intruder enters the ownship's collision envelope. The dimensional parameters of the envelope are defined as

$$\begin{cases} L_{en} = R_{wc} + L_{un}^{o} + L_{un}^{i} \\ H_{en} = H_{wc} + H_{un}^{o} + H_{un}^{i} \end{cases} \tag{6}$$

where (L_{en}, H_{en}) represents the radius and half the height of the collision envelope, respectively, which consists of the maximum length of the DWC in the horizontal and vertical projection (R_{wc}, H_{wc}), the flight uncertainty area of the ownership (L_{un}^{o}, H_{un}^{o}) and the intruder (L_{un}^{i}, H_{un}^{i}).

The maximum length of DWC is defined as $R_{wc} = 2000$ ft, $H_{wc} = 250$ ft referring to the DWC volume in Cone et al. (2019). When defining the DWC separation, the influence of wind on aircraft is an overlooked factor. Therefore, this study introduces an uncertainty area as a virtual extension of the original DWC range, capturing the positional uncertainty caused by wind effects during operation.

3.2. MAC probability assessment for cooperative UAS

This section models the MAC probabilities for cooperative UAS. First, we introduce how to assess the conflict probability during encounters, which is the strategic mitigation failure. Then we elaborate an approach time estimation model to determine the effectiveness of tactical mitigation. Finally, the probability of collision avoidance failure will be characterized by the failure rate of the DAA system.

3.2.1. Strategic mitigation failure probability

The conflict probability estimation model is based on the acquired flight trajectories, aiming to characterize the strategic mitigation failure due to uncertainty factors, which can be divided into three steps. Firstly, the trajectory of the aircraft during the encounter needs to be predicted, and the detailed flight plan can be obtained from the low-altitude service provider, so it is not covered in the model. Secondly, the uncertainty in these trajectories is estimated, covering lateral, longitudinal, and vertical errors. The third step, which is the subject of this part, is to estimate the conflict probability by deriving an analytical solution in three dimensions.

The trajectory error can be expressed as the offset of the aircraft's true position relative to the original trajectory. According to the performance-based navigation (PBN) manual in Fellner and Konieczka (2019), the primary cause of the offset is attributed to the total system error (TSE), which is the sum of the navigation system error (NSE), the flight technical error (FTE), and the path definition error (PDE). The PDE is the difference between the defined path and the desired path, which is usually negligible. In addition, wind drift is inherently a component of FTE, but considering strong wind conditions, it is reasonable to increase the FTE to reflect the additional error introduced by wind effects, which is called the wind error (WDE). In the model, the trajectory error is assumed to follow a Gaussian distribution with zero mean and covariances in the lateral, longitudinal, and vertical directions. Based on previous studies, we have determined the standard deviations of these error distributions, as shown in Table 4. The results show that the FTE error in the longitudinal direction increases with the time of flight. Therefore, the projection of the total error horizontally takes the form of an ellipse, which follows a Gaussian distribution with variance $\mathrm{TSE} = \sqrt{\mathrm{NSE}^2 + \mathrm{FTE}^2 + \mathrm{WDE}^2}$.

Assuming $(\sigma_1^2, \sigma_2^2, \sigma_3^2)$ are the standard deviations of the predicted position and R is the rotation matrix from body axis system to global coordinate system, the error covariance of an aircraft in the body axis system is $S = \mathrm{diag}(\sigma_1^2, \sigma_2^2, \sigma_3^2)$, and in the global coordinate system it is $K = RSR^T$. Let the subscripts o and i represent the ownship and intruder, respectively, the two error covariances of an aircraft pair are combined into a single equivalent covariance represented as $M = K_o + K_i$, which is assigned to the intruder. The collision envelope is assigned to the owner so that it can be considered as a zero uncertainty, as shown in Fig. 4. From a horizontal perspective, at the moment of an aircraft pair encounter, the collision envelope is a circle, and the combined error is a probability density function that can be represented as a surface over the ellipse, the total volume under the surface is unity. However, the real goal of this part is to calculate the total mitigation failure probability during encounter, rather than the instantaneous probability. Therefore, the collision envelope is projected along a line parallel to the relative velocity to form an extended collision zone, the length of which is calculated based on the distance between the current position of the ownship and the position after the ownship fly at the relative speed for 25 s, plus the value of L_{en}. The failure probability is equal to the portion of the probability density surface that falls within this extended collision zone, as shown in Fig. 4. Then the coordinate transformation will be presented to determine the analytical solution of this probability.

Let p and q represent the original and transformed coordinates, respectively. A linear coordinate transformation is $q = Tp$, where T is a transformation matrix which needs to be determined. If $W = T^{-1}$, then p

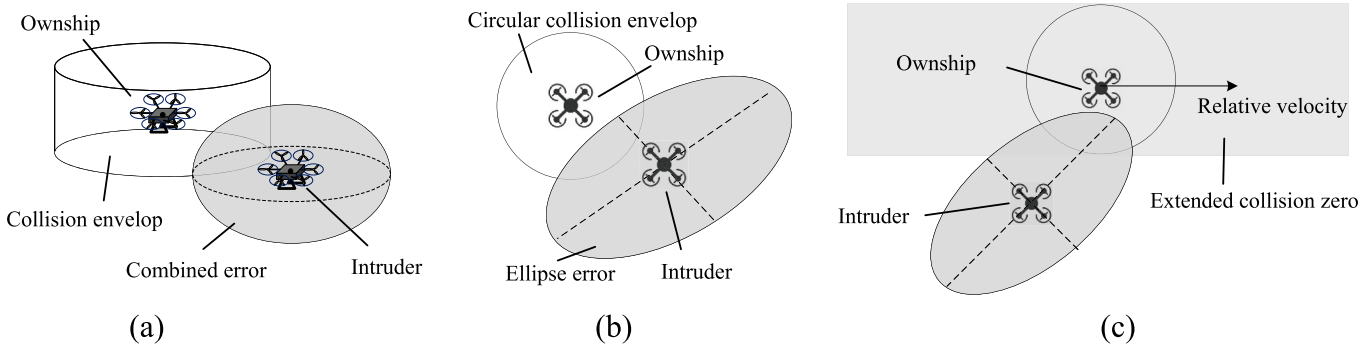


Fig. 4. Relative geometry of an ownship–intruder encounter.

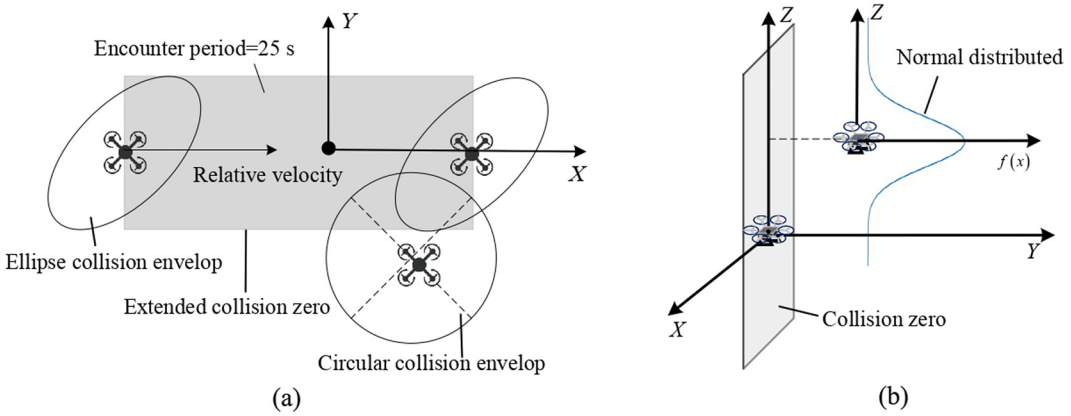


Fig. 5. Transformed encounter geometry.

$= Wq$. In the transformed coordinate system, the combined error covariance is $Q = TMT^T$, where the combined error covariance M can be represented as $M = LL^{-1}$ according to Cholesky decomposition and L is lower triangular. Let H represent the orthogonal rotation matrix, so $HH^T = I$, if $H = TL$, then:

$$Q = TMT^T = TL(TL)^T = HH^T \tag{7}$$

Through coordinate transformation, the error ellipsoid is converted into the standard form of a unit sphere, which allows for decoupling. Consequently, the circular cylinder becomes an elliptical cylinder. This study assumes that during the encounter, both aircraft remain in level flight with constant relative velocity and direction. As a result, horizontal and vertical motions are independent, and the above transformations can be decoupled into two-dimensional and vertical conflict probabilities through simple scaling, as shown in Fig. 5. Analytical solutions are then derived for both directions, and the total conflict probability is obtained as the product of the two because of their independence.

For horizontal probability, first, using the rotation matrix H mentioned in Eq. (7) rotate the transformed coordinate system so that the relative velocity is the x-direction of the coordinate system. If $\Delta v = v_i - v_o$ is the relative velocity, the new relative velocity after the coordinate transformation is $\Delta\bar{v} = T\Delta v = HL^{-1}\Delta v$, and the partial velocity $\Delta\tilde{v}$ in the transformed coordinate system can be represented as $\Delta\tilde{v} = L^{-1}\Delta v = \left[\Delta v_x, \Delta v_y\right]^T$. According to $HH^T = I$, the rotation matrix H can be represented as

$$H = \frac{1}{\|\Delta\tilde{v}\|}\begin{bmatrix}\Delta v_x & \Delta v_y \\ -\Delta v_y & \Delta v_x\end{bmatrix} \tag{8}$$

Then, determine the integral expression of the 2-D conflict probability and calculating the upper and lower bounds. The boundary on the y-axis is the maximum and minimum value of the elliptical boundary. Let Δy_{pc}, Δy_{qc} represent the boundary distance of y-axis in the original and transformed coordinate systems, then:

$$\|\Delta p_c\| = \|W\Delta q_c\| = 2L_{\text{en}} \tag{9}$$

where $W = T^{-1} = LH^{-1}$, Eq. (9) can be expanded according to

$$W^T W = \begin{bmatrix}x_1 & x_2 \\ x_2 & x_3\end{bmatrix} \tag{10}$$

where x_1, x_2, and x_3 are the matrix elements.

Setting the discriminant of that quadratic equation to zero and solving for Δy_c. The boundary distance of x-axis Δx_c is equivalent to the distance of the aircraft pair flying during encounter, as shown in Eq. (11):

$$\begin{cases}\Delta y_c = \pm 2\cdot L_{\text{en}}\sqrt{x_1/\left(x_1x_3 - x_2^2\right)} \\ \Delta x_c = d_{sr} = \Delta v\cdot t_{\text{warning}} + L_{\text{en}}\end{cases} \tag{11}$$

where d_{sr} is the relative distance traveled between the two aircraft over a 25-s interval. The horizontal probability P_{hor} can be expressed as follows by secondary decoupling

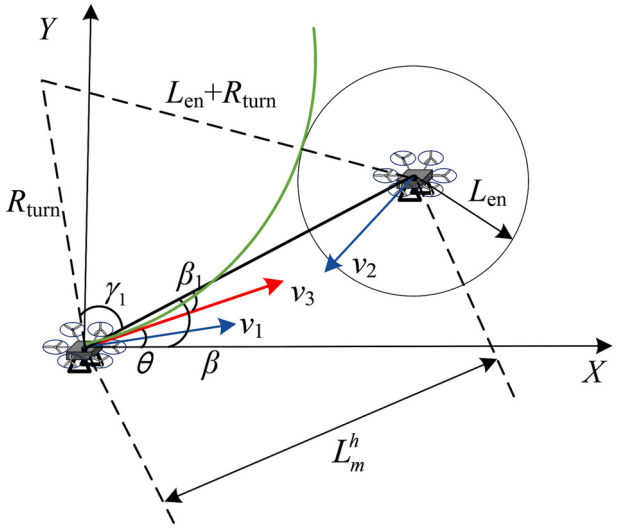


Fig. 7. Process of heading adjustment.

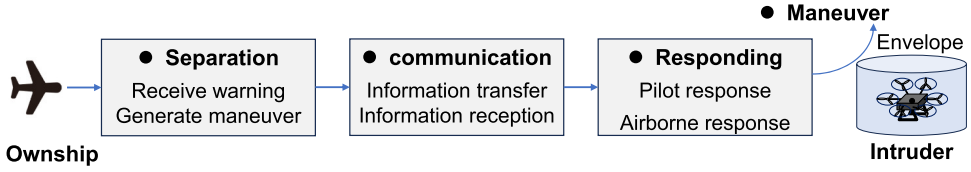


Fig. 6. General process of tactical mitigation.

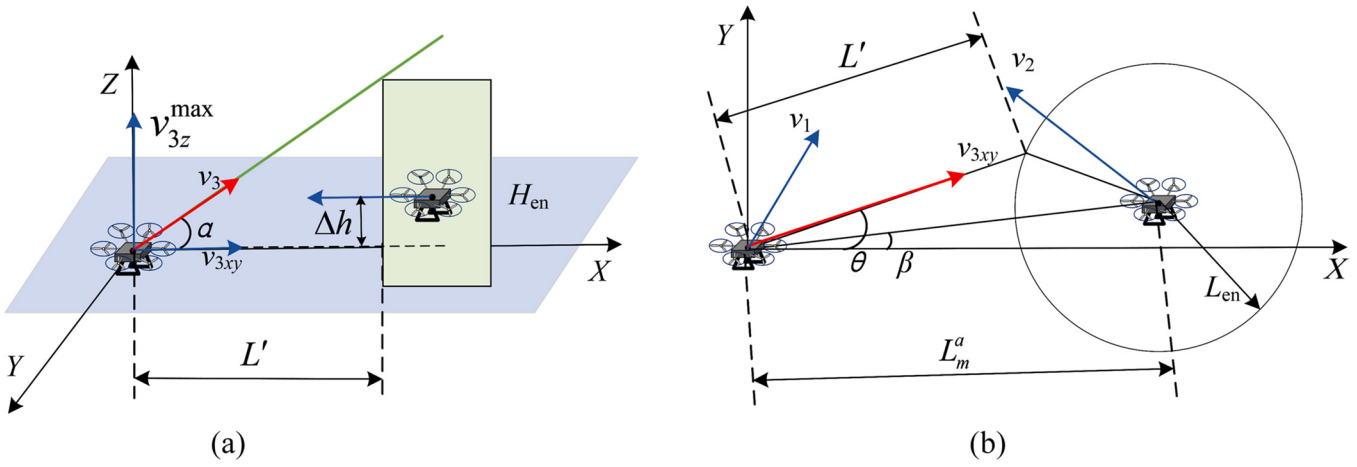


Fig. 8. Process of altitude adjustment.

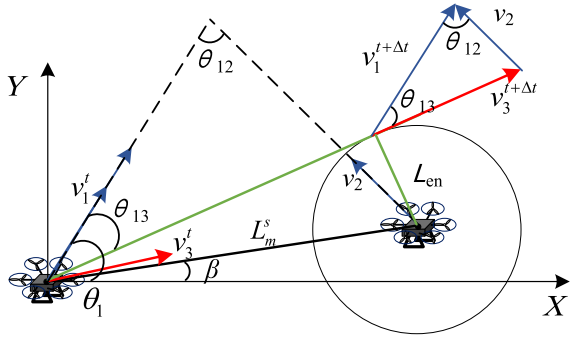


Fig. 9. Process of speed adjustment.

$$P_{hor} = \int_{-\Delta x}^{-\Delta x+\Delta x_c} p(x)\mathrm{d}x \int_{-\Delta y-\frac{\Delta y_c}{2}}^{-\Delta y+\frac{\Delta y_c}{2}} p(y)\mathrm{d}y \tag{12}$$

where Δx_c and Δy_c represent the initial distances between the aircraft in the transformed coordinate system, $p(x)$ and $p(y)$ are standard normal distributions.

The vertical conflict probability corresponds to the integral of the one-dimensional normal distribution over the conflict zone:

$$P_{ver} = \int_{\frac{-H_{en}-\Delta z}{\sigma_3}}^{\frac{H_{en}-\Delta z}{\sigma_3}} p(z)\mathrm{d}z \tag{13}$$

where Δz denotes the z-coordinate of the intruder with respect to the ownship, σ_3 is the standard deviation of the error, $p(z)$ represents the standard normal distribution.

The conflict probability during encounter (strategic mitigation failure) is

$$P_{ST}^{cop} = P_{hor} \cdot P_{ver} \tag{14}$$

3.2.2. Tactical mitigation failure probability

Once strategic mitigation fails, the ownship is responsible for executing a tactical avoidance maneuver upon encountering an intruder, triggered by a warning issued after the strategic failure. The formulation of strategic and tactical measures is the responsibility of different entities. The party executing tactical mitigation does not know the actual position of the aircraft caused by environmental errors. Therefore, strategic and tactical mitigation measures are assumed to be independent, and tactical mitigation is still carried out based on the original positional relationship in the flight plan. Moreover, the tactical mitigation considers multiple maneuvers, but only a single optimal maneuver is selected for execution, without considering combinations of maneuvers.

This section presents a maximum approach time estimation model to characterize tactical mitigation failure, which is defined to occur if a loss of well clear (LOWC) happens. The probability assessment is carried out in two steps: Firstly, determining the latency time by analyzing the tactical mitigation process. Secondly, calculating the minimum distance required for maneuvering and the maximum approach time from warning reception to the latest possible execution of the maneuver. If the latency time exceeds the maximum approach time, meaning that the ownship cannot avoid the LOWC no matter what maneuvers it takes, then the tactical mitigation failure probability can be expressed as

$$P_{TC-ST}^{cop} = 1 - \phi(t_{ap}) \tag{15}$$

where $\phi(t)$ is the cumulative distribution function of latency time, and the variable t_{ap} represents the maximum approach time.

The latency time is determined by analyzing the tactical mitigation process, as shown in Fig. 6. Specifically, after receiving strategic mitigation failure, the USSP generates and transmits appropriate avoidance instructions to the ownship. Following instruction, the pilot responds to the specified maneuver to prevent LOWC, and then the aircraft starts to perform a maneuver to avoid LOWC. Latency time is defined as the cumulative duration of three sequential phases: separation computation, instructions communication, and response implementation. Assuming μ_{sep}, μ_{com}, μ_{pil} stand for the expectations of them and σ_{sep}, σ_{com}, σ_{pil} represent standard deviations, the values have shown in Table 5. The latency time is subject to a normal distribution with exception $\mu_{ta} = \mu_{sep} + \mu_{com} + \mu_{pil}$ and deviation $\sigma_{ta} = \sqrt{\sigma_{sep}^2 + \sigma_{com}^2 + \sigma_{pil}^2}$, the cumulative

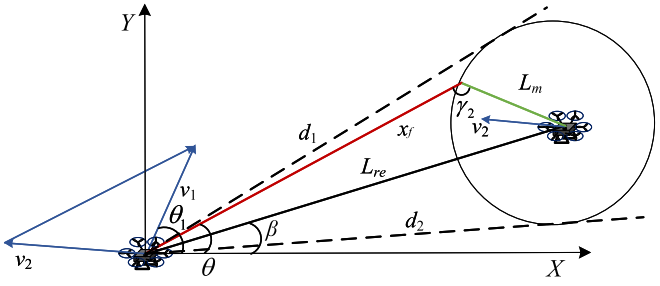


Fig. 10. Positional relationship of ownship and intruder when tactical mitigation.

distribution function is

$$\phi(t) = \frac{1}{2}\left(1 + \mathrm{erf}\left(\frac{t-\mu_{\mathrm{ta}}}{\sqrt{2}\,\sigma_{\mathrm{ta}}}\right)\right) \tag{16}$$

The approach time is the time taken by the ownship from receiving warning to the latest time of taking maneuver. Obviously, the shorter distance required for an ownship to perform avoidance maneuvers, the longer it is allowed to fly after warning, so it is necessary to calculate the minimum maneuvering distance before determining the maximum approach time.

The maximum approach time estimation model considers multiple maneuvers, including heading, altitude and speed adjustment, to calculate the maneuver distance more objectively and extend its application scope to 3-D space. The maneuver with the shortest distance is considered the optimal maneuver, so the distance is defined as the minimum maneuvering distance L_{m}, and the allowable flight time is the maximum approach time t_{ap}. Figs. 7–9 show the processes of maneuvering with the collision envelope centered on the intruder, the model is based on a coordinate system with the *y*-axis as the north-direction and the *x*-axis as the reference base direction.

For heading adjustment, it is considered that the aircraft can take the maximum inclination angle $\varphi_{\max}$ to make a turn, then the maximum lateral turn overload n and the minimum turn radius R_{turn} can be calculated from Eq. (17), in that ω is the angular velocity, v_l is the relative linear velocity.

$$\begin{cases} ng = g\cdot\tan(\varphi_{\max}) \\ R_{\mathrm{turn}} = \dfrac{v_l}{\omega} = \dfrac{v_l^2}{ng} \end{cases} \tag{17}$$

When the trajectory of the ownship turning with the minimum radius R_{turn} is tangent to the collision envelope, as shown in Fig. 7, the distance of the ownship from the intruder L_m^h is defined as the minimum maneuvering distance under heading adjustment. Assuming the direction of relative velocity v_3 is θ, the azimuth of two aircraft is β, so the angle between azimuth and relative velocity can be obtained by $\beta_1 = |\beta - \theta|$. According to cosine theorem, the minimum maneuvering distance L_m^h can be calculated from a triangle with the top angle is γ_1, the top angle varies according to the θ, if $\theta > \beta$, then $\gamma_1 = \pi/2 + \beta_3$, if $\theta \le \beta$, then $\gamma_1 = \pi/2 - \beta_3$, as shown in Eq. (18).

$$\cos\gamma_1 = \frac{R_{\mathrm{turn}}^2 + {L_m^h}^2 - (R_{\mathrm{turn}} + L_{\mathrm{en}})^2}{2R_{\mathrm{turn}}\cdot L_m^h} \tag{18}$$

For altitude adjustment, it is considered that the aircraft will rise quickly at the maximum climb speed $v_{3z}^{\max}$ to avoid LOWC with the intruder, assuming that the horizontal relative velocity v_{3xy} remains constant during climbing, the climb angle α can be calculated by $\alpha = \arctan\left(v_{3z}^{\max}/v_{3xy}\right)$.

Fig. 8 shows the vertical and horizontal perspective during the adjustment process, L' indicates the shortest distance to the collision envelope, and Δh indicates the altitude difference between ownship and intruder. In the right triangle, the L' can be calculated from Eq. (19). For the horizontal perspective, the length of the position line between ownship and intruder is exactly the minimum maneuvering distance L_m^a, which is shown in Eq. (20):

$$L' = (H_{\mathrm{en}} + \Delta h)\cdot\frac{v_{3xy}}{v_{3z}^{\max}} \tag{19}$$

$$\cos(|\beta - \theta|) = \frac{{L_m^a}^2 + L'^2 - L_{\mathrm{en}}^2}{2L'\cdot L_m^a} \tag{20}$$

For speed adjustment, assuming the ownship avoids collision with an intruder by accelerating, the critical condition for LOWC is that the relative velocity is precisely tangent to the collision envelope, as illustrated in Fig. 9. In other words, if the ownship's velocity decreases slightly, the relative velocity will intersect with the collision envelope, leading to the occurrence of LOWC. Define the convergence angle of the aircraft pair as θ_{12}, the initial velocity of the ownship as v_1^t. If the acceleration process is ignored, the ownship can reach its maximum velocity $v_1^{\max}$ at the critical moment. At this instant, the relative velocity $v_3^{t+\Delta t}$ can be determined using a special triangle, allowing one of its angles to be further derived, as shown in Eq. (21):

$$\begin{cases} v_3^{t+\Delta t} = \sqrt{\left(v_1^{\max}\right)^2 + v_2^2 - 2v_2 v_1^{\max}\cos\theta_{12}} \\ \theta_{13} = \arcsin\left(\dfrac{\sin\theta_{12}\cdot v_2}{v_3^{t+\Delta t}}\right) \end{cases} \tag{21}$$

The shortest distance can be derived from the left triangle in Fig. 9, where β is the angle between the position line and the *X*-axis, θ_1 is the heading angle of the ownship. By incorporating the collision envelope, the minimum maneuvering distance L_m^s can be shown as

$$L_m^s = \frac{l_{\mathrm{en}}}{\sin(\theta_1 - \beta - \theta_{13})} \tag{22}$$

Based on the minimum maneuvering distance obtained by the above maneuvers, the approach time t_{ap} can be calculated from Fig. 10. The

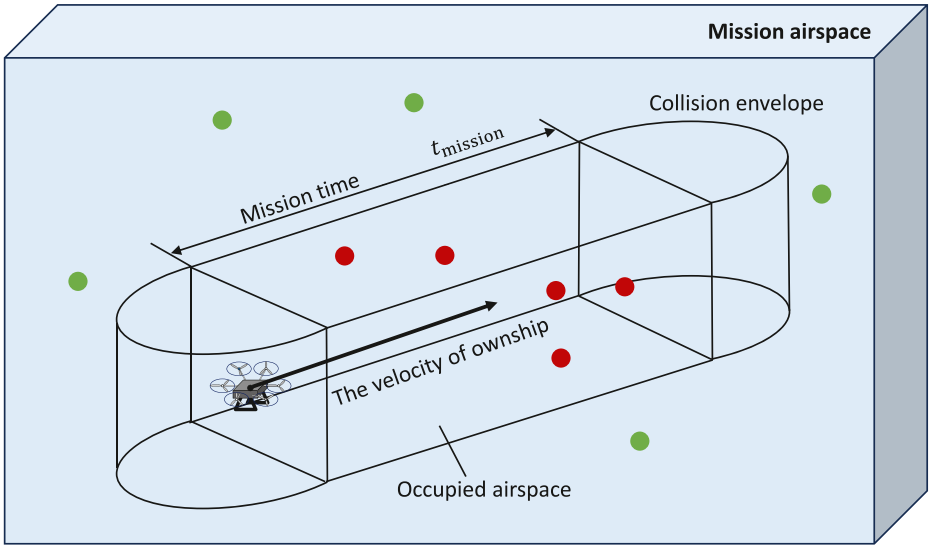


Fig. 11. Dynamic gas model for non-cooperative UAS.

relationship between the two velocity vectors is an triangular, in which the direction of relative velocity θ can be obtained. A conflict is only possible if the relative velocity v_3 is within a certain range that between two tangent lines d_1 and d_2 as shown in Fig. 10. The maximum and minimum θ can be calculated from $\Delta\theta = \arcsin(L_m/L_{re})$ and Eq. (23):

$$\begin{cases} \theta_{\min} = \beta - \Delta\theta \\ \theta_{\max} = \beta + \Delta\theta \end{cases} \tag{23}$$

The relationship between relative distance and allowable approach distance can also be described by the triangle. The relative distance L_{re} and the maneuvering distance L_m is known, so the remaining angle γ_2 can be calculated by Eq. (24):

$$\gamma_2 = \arcsin\left(\frac{L_{re}}{L_m}\sin(\theta - \beta)\right) \tag{24}$$

The cosine theorem is then used to calculate the approach distance x_f:

$$x_f = \sqrt{\left(L_m^2 + L_{re}^2 - 2L_m L_{re}\cos[\pi - (\gamma_2 + \theta - \beta)]\right.} \tag{25}$$

Obviously, the x_f is a function of the maneuver distance L_m, so maximum allowable approach time t_{ap} can be expressed as

$$t_{ap} = \frac{\max\{x_f(L_m^h), x_f(L_m^a), x_f(L_m^s)\}}{v_3} \tag{26}$$

where $x_f(L_m^h)$, $x_f(L_m^a)$, and $x_f(L_m^s)$ represent the maneuvering distance under different strategies. v_3 represents the relative velocity.

3.2.3. Collision avoidance failure probability

After tactical mitigation fails, the ownship needs to perform collision avoidance against intruders, which mainly depends on the DAA systems. We regard collision avoidance failures $P_{\text{CA-TC}}^{\text{cop}}$ as the risk ratio associated with the DAA system, these probabilities are bounded by the ASTM International (2020), which specifies performance requirements for small UAS DAA systems. For analysis, we adopt the upper bound as the collision avoidance failure probability, namely 0.18 for intruders equipped with a transponder. Since the specification explicitly assumes that aircraft does not rely on air traffic control separation services when executing DAA instructions, the DAA system is expected to operate independently after tactical mitigation fails, and the safety layers associated with these measures are considered independent.

3.3. MAC probability assessment for non-cooperative UAS

3.3.1. Procedure mitigation failure probability

Beyond cooperative UAS, the ownship may face another risk of illegal intrusions from non-cooperative UAS, which also can lead to MAC accidents. At present, the risks from non-cooperative UAS are mainly prevented by procedural mitigation measures, such as dynamic corridor design. Due to the plans and trajectories of intruding UAS cannot be easily determined, it is difficult to calculate the failure probability of procedural mitigation numerically as the above method. While the gas model offers a solution by simulating air molecule distribution to quantify UAS collision risks from an airspace perspective. The traditional gas model only assesses risk based on the positional distribution of air molecules without considering their mobility, which is obviously not consistent with the motion characteristics of aircraft. Therefore, we propose a dynamic gas model by considering the velocity of ownship.

The dynamic gas model first establishes the airspace occupied by ownship during the flight, which is an approximate cube determined by the collision envelope mentioned in Section 3.1, the velocity of ownship, and the flight time. Then this model considers that the intruder's position follows a uniform distribution during ownship's mission execution, and there is no movement trend within an instant. The procedure mitigation will be regarded as a failure if an intruder enters the occupied airspace, as shown in Fig. 11, where red dots are conflicting intruders and green dots represent non-conflicting intruders. The occupied airspace can be represented as

$$A_{\text{oc}} = 2H_{\text{en}}(\pi \cdot L_{\text{en}}^2 + v_1 \cdot t_{\text{mission}}) \tag{27}$$

where L_{en} and H_{en} are the dimension parameters of the collision envelope, and v_1 and t_{mission} represent the velocity and the flight time of ownship.

The logic for determining a UAS intrusion is defined in Eq. (28). The variable f_{in}^j indicates whether the j-th intruder has affected the ownship. When the intruder enters the occupied airspace, a collision risk exists, i.e., $f_{\text{in}}^j = 1$; otherwise, $f_{\text{in}}^j = 0$. Here, (x_j', y_j', z_j') denotes the location of the

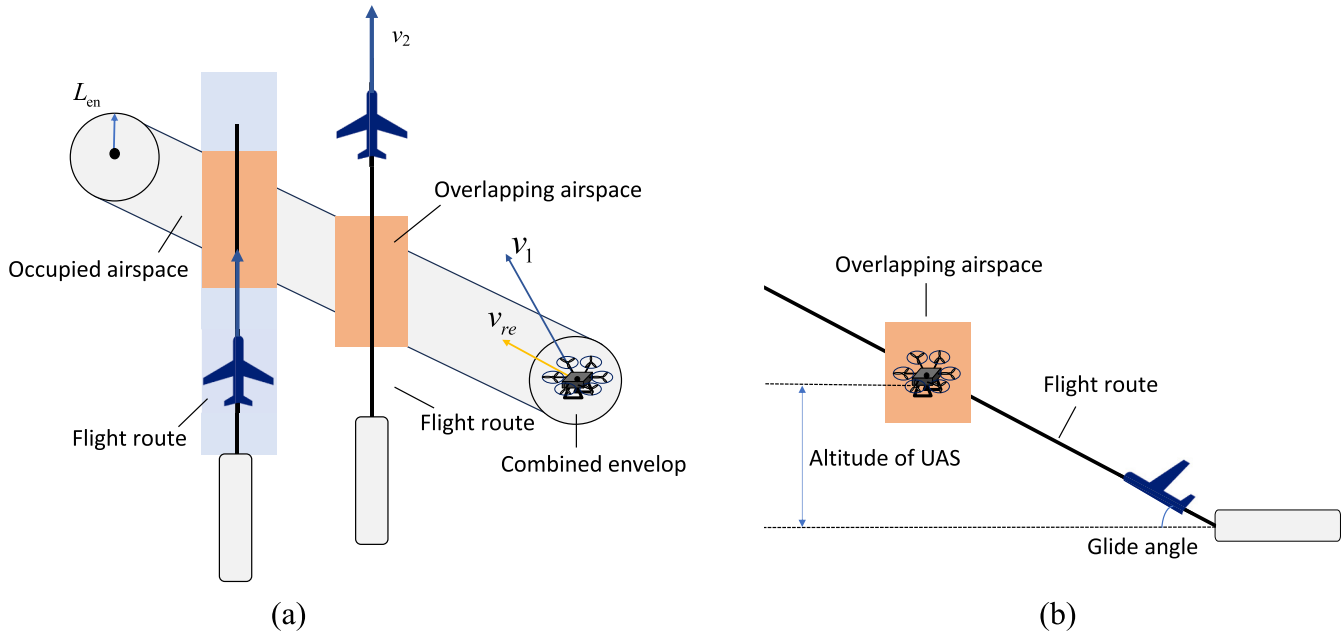


Fig. 12. Dynamic gas model for manned aircraft.

UAS.

$$f_{\text{in}}^{j} = \begin{cases} 1 \cdots (x_j', y_j', z_j') \in A_{\text{oc}} \\ 0 \cdots (x_j', y_j', z_j') \notin A_{\text{oc}} \end{cases} \tag{28}$$

The procedure mitigation failure of non-cooperative UAS can be calculated from Eq. (29):

$$P_{\text{PC}}^{\text{non-cop}} = \frac{\sum_{1}^{N_{\text{uas}}} f_{\text{in}}^{j}}{N_{\text{uas}}} \tag{29}$$

where N_{uas} represents the estimated total number of noncooperative UAS in a certain period, which can be obtained by analyzing historical data. f_{in}^{j} determines whether the j-th intruder has a collision risk.

3.4. MAC probability assessment for manned aircraft

The airport area is a strictly controlled zone, but within the integrated airspace, the UAS corridor may intersect with the operational area of manned aircraft. Temporal separation is designed to prevent them from occupying the same space simultaneously. However, the untimely opening of corridors due to human error can result in overlapping operations, increasing the likelihood of manned aircraft encroaching into UAS corridors. Given this risk, it is crucial to assess the probability of collisions involving manned aircraft.

Since the operational range of the ownship is primarily below 1000 m, the highest risk of collision arises during the approach and departure phases of manned aircraft. To assess the collision risk, we refer to the approach and departure procedures and the layout of the airport runway to establish an alert area, so called the SID and STAR area. If the flight trajectory of an ownship passes through the SID and STAR area, the probability of an encounter with manned aircraft must be assessed based on the flight's operation information, which is the procedural mitigation failure probability assessment. Then a maneuver instruction is issued to the ownship to facilitate avoidance, serving as a tactical mitigation measure, and the failure probability of this process also needs to be assessed.

3.4.1. Procedure mitigation failure probability

Unlike non-cooperative UAS, the approach and departure of a manned aircraft strictly follow a specific flight plan, and its distribution in terminal area depends on the structural characteristics of the flight routes. However, the exact position of the manned aircraft in routes is difficult to obtain during the flight period, and it exhibits great uncertainty according to the flight plan made every day. Therefore, the distribution of manned aircraft inside the flight route can be considered as random, similar to air molecules. We establish a gas model based on the structure of approach and departure routes to assess the probability of encounter with a manned aircraft when entering the SID and STAR area, i.e., the procedure mitigation failure probability.

In the gas model, the ownship is represented as a mass enclosed within a combined envelope, where the total volume is the sum of the respective envelopes of both aircraft. The area swept by the ownship at a certain time with combined envelope can be approximated as a cube, referred to as the occupied airspace. Manned aircraft in terminal airspace follow fixed paths with minimal deviation, so their center is assumed to align with the approach and departure routes. As illustrated in Fig. 12, the gray area represents the occupied airspace of the ownship during its mission. A potential encounter with a manned aircraft occurs when the cube-shaped occupied airspace overlaps with the flight routes in both the horizontal and vertical dimensions. This region, shown in orange in Fig. 12, is termed the overlapping airspace. According to the gas model, a manned aircraft is treated as an air molecule uniformly distributed along the flight route. If it enters the overlapping airspace, an encounter is deemed to have occurred. In summary, the key task is to determine the length of the approach and departure routes that are at risk of collision, specifically, the segments that intersect with the occupied airspace. This is achieved by identifying the intersection points between the approach and departure routes and the cube-shaped occupied airspace, then calculating the distance between them.

Based on the above analysis, assuming the airport has m runways, the total number of manned aircraft present at a given time when the ownship crosses runway j is N_{man}^{j}. According to the gas model, these aircraft are assumed to be uniformly distributed along the fixed flight route. The procedural mitigation failure of manned aircraft can be calculated from Eq. (30):

$$p_{\text{PC}}^{\text{man}} = 1 - \prod_{j=0}^{m} \left(1 - N_{\text{man}}^{j} \cdot \frac{S_{\text{oc}}^{j}}{S_j}\right) \tag{30}$$

where S_{oc}^{j} is the length of approach and departure routes corresponding to runway j in the occupied airspace, and S_j is its total length.

3.4.2. Tactical mitigation failure probability

When the procedure mitigation with manned aircraft fails, the ownship immediately executes tactical mitigation measures and takes appropriate actions to avoid the SID and STAR area. Due to the large speed of manned aircraft, the effect of altitude and speed adjustment is not obvious, so the ownship mainly uses the heading adjustment to avoid entering the SID and STAR area to mitigate the MAC risk. When the ownship approaches this area, the minimum maneuvering distance for collision avoidance is obtained by the positional relationship between ownship and the boundary of SID and STAR area, which is then combined with the latency time to calculate the tactical mitigation failure probability with manned aircraft. This process is similar to that shown in Fig. 10, and the relevant model has been described in detail in Section 3.2.2.

Table 3
Aircraft parameters in the simulation.

Parameter	Length (m)	Height (m)	Climb (m/s)	Cruise (m/s)	Range (km)
EHang 216	3.86	1.76	10	25	35
DJI Mavic3	0.34	0.15	8	15	28

Table 4
Environmental error parameters in the simulation.

Parameter	Lateral deviation	Vertical deviation	Growth rate
Wind error	3.7 m	3.7 m	—
NSE	8 m	5 m	—
FTE	3.2 m	2.3 m	0.62 m/s

Table 5
Latency parameters in the simulation.

Parameter	Separation	Communication	Pilot + heading adjusting	Pilot + altitude adjusting
μ (Mean)	6.9	2.76	4.77	2.63
σ (Deviation)	2.45	1.18	3.11	1.91

4. Monte Carlo simulation validation

The MAC probability assessment model in this study considers four main components: the procedural mitigation failure, the strategic mitigation failure, the tactical mitigation failure, and the collision avoidance failure. For procedural mitigation failure $P_{\text{PC}}^{\text{non-cop}}$ or $P_{\text{PC}}^{\text{man}}$, the assessment models are constructed based on the widely used gas model. Lum and Waggoner (2011) have demonstrated that, in most cases, evaluating the

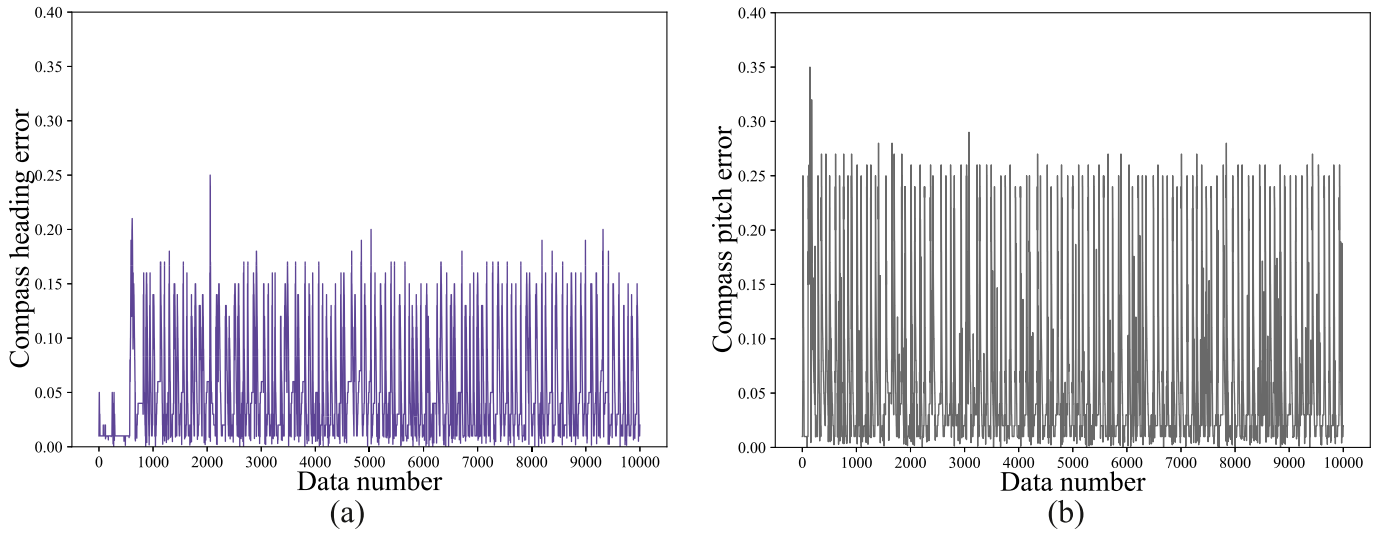


Fig. 13. Sensor error parameters in the database.

collision effects referring to the motion of random gas molecules is a fairly representative task. The assessment of collision avoidance failure $P_{\text{CA-TC}}^{\text{cop}}$ comes from the performance requirements specification of the DAA system. The core of this section is to validate the accuracy of strategic, tactical mitigation failure models and the entire MAC assessment timeline.

The validation process is based on Monte Carlo simulations under the following assumptions: (1) During the approach of the ownship and the intruder, both aircraft remain in level flight, with constant relative velocity and direction. (2) The ownship is responsible for performing the avoidance maneuver when encountering an intruder. (3) When executing a collision avoidance maneuver, only one optimal strategy is selected, and combinations of multiple strategies are not considered in this study.

Accordingly, three types of Monte Carlo simulations are designed: result-oriented, process-oriented, and comprehensive simulation. The strategic mitigation failure model relies on deterministic prediction, meaning that the spatial positions of aircraft can be precisely obtained from the flight plan. The conflicts are mainly due to various errors during encounters, and we regard the maximum error in that process as the final error. As a result, there is no need to simulate the entire flight process—only the final spatial positions of the aircraft and their associated errors need to be set in the simulation scenario. This approach is referred to as result-oriented Monte Carlo simulation. Conversely, tactical mitigation failures are primarily caused by various in-flight latencies. To accurately capture these effects, it is essential to design a simulation scenario that accounts for the entire encounter process of aircraft pairs. This approach is known as process-oriented Monte Carlo

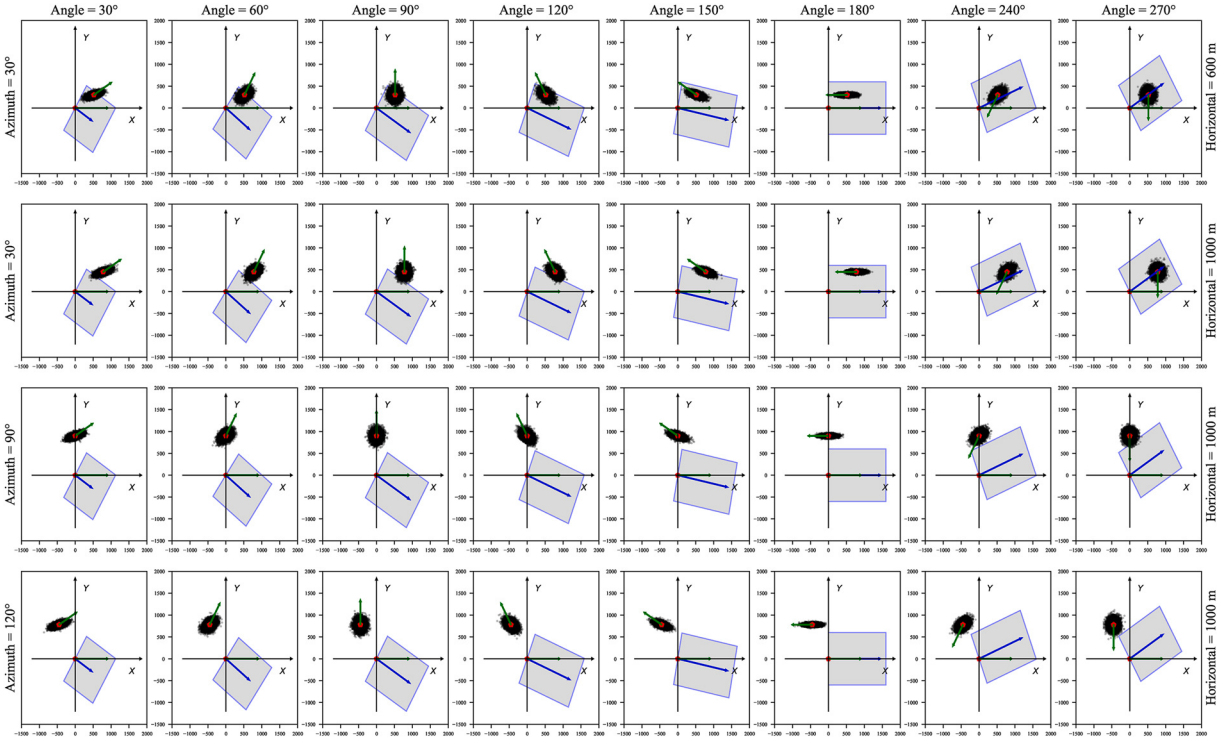


Fig. 14. Result-oriented Monte Carlo experiment with vertical separation of 0 m.

simulation. The comprehensive simulation is used to validate the complete MAC risk assessment process for the ownship facing cooperative UAS, assuming mitigation measures operate independently during the MAC assessment. The simulation parameters are shown in Section 4.1, and the setup and comparative results are analyzed in Sections 4.2, 4.3, and 4.4.

4.1. Simulation parameter

4.1.1. Aircraft parameter

The simulation parameters mainly include the aircraft parameters, the environment parameters, and the latency parameters. In the Monte Carlo simulation, a typical air taxi EHang 216 eVTOL is chosen as the ownship; the intruder is regarded as a Mini UAS performing an aerial photography task. The detailed parameters are shown in Table 3.

4.1.2. Environment parameter

The environmental parameters mainly refer to various errors, which are used to characterize the position uncertainty of aircraft in the strategic mitigation and tactical mitigation phase, including wind error, NSE, and FTE. The wind error is based on the results in the Federal Aviation Administration (1988); Hongsheng et al. (2011), which analyze the position error during turbulence-disturbed approach operations with an upper bound of 4.5–7.4 m. The estimation of the NSE follows the International Organization for Standardization (ISO) standard proposal 24355 for the performance requirements of a GNSS for the multi-rotor UAS. This proposal estimates a value of 10 m for the horizontal error, which is similar to the 16 m defined in the International Organization for Standardization (ISO) (2023), where the vertical error is defined to a range of 8–10 m depending on the approach types. The vertical error will be estimated to a conservative value of 10 m in this study. Currently, there are no standard requirements for FTE with UAS, but previous studies have documented a series of flight tests conducted in open fields to assess FTE deviations in the along-track (longitudinal), cross-track (lateral), and vertical (height) directions (Pang et al., 2022; Wang et al., 2021). The results indicate that while the lateral and vertical FTE errors remain nearly constant during UAS operation, the longitudinal error increases over time. Based on previously introduced considerations and a 95% confidence interval, Table 4 summarizes the proposed σ values and growth rates of these errors. The uncertainty region of the collision envelope is primarily influenced by wind during operation, with its magnitude defined as the 2σ values of the wind error.

In order to be closer to the actual mission flight simulation, sensor errors, including compass heading error and compass pitch error caused by vibration, are incorporated. The sensor error in the Monte Carlo simulation is generated through the software in the Loop (SITL) simulator in the Ardupilot flight Control firmware. In the SITL, by sending the random flight plans to the virtual Pixhawk flight controller, the virtual UAS is guided to finish the corresponding flight and save the simulation log of each flight. After a number of simulated mission flights, 20,000 sets of necessary sensor errors are extracted from the simulation logs to form a pre-defined database, as shown in Fig. 13. In the process-based Monte Carlo simulation, at each time step, the compass heading error and compass pitch error are randomly sampled from the database and incorporated into the original trajectory data to simulate the uncertainty in executing the collision avoidance maneuver.

4.1.3. Latency parameter

The latency parameter is mainly used in the tactical mitigation phase to simulate the cumulative distribution function shown in Eq. (16). There are three categories of latency time: separation, communication, and responding. The values of these parameters are shown in Table 5 according to previous research (Vila Carbó et al., 2023). It is worth mentioning that the response times of pilots vary depending on different maneuvers according to the experimental results performed by the Shively et al. (2013), which is consistent with the idea of estimating the approach time based on multiple maneuvers in this study.

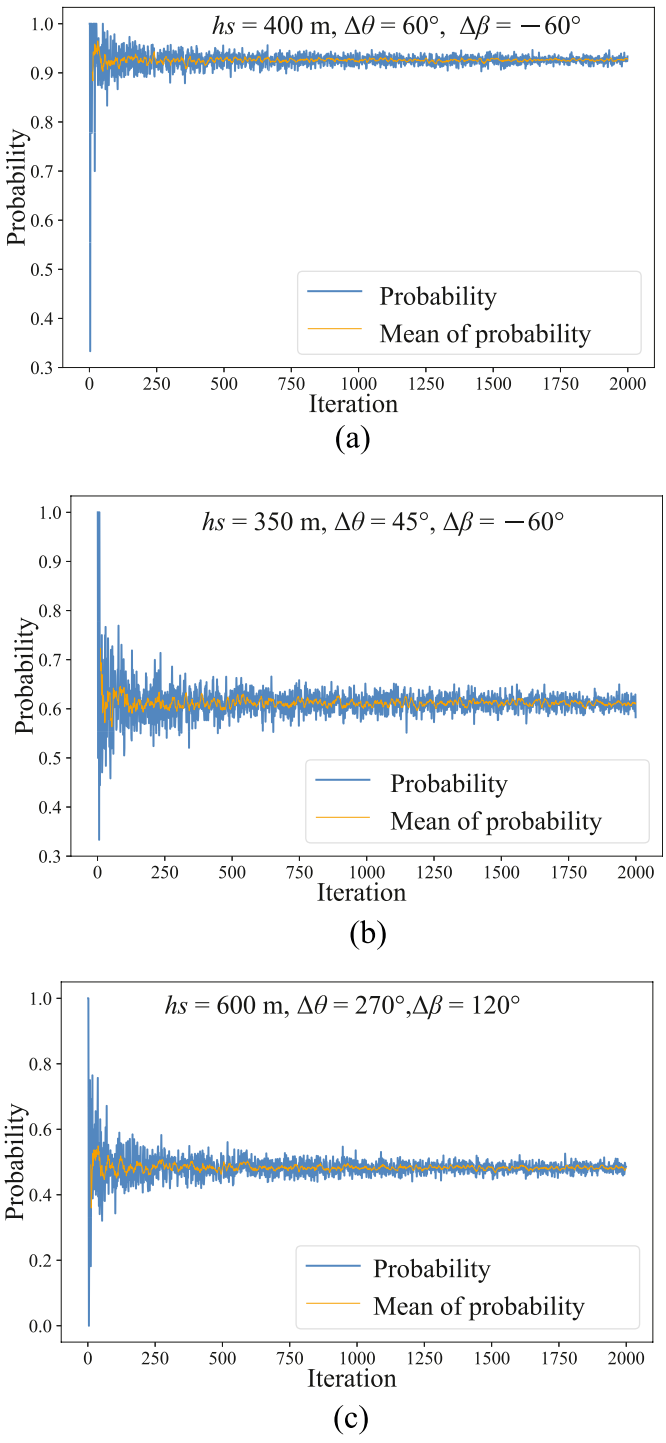


Fig. 15. Relationship between the probability calculated by result-oriented Monte Carlo simulation and the number of iterations.

4.2. Result-oriented simulation for validating strategic mitigation failure

4.2.1. Simulation setup

The verification is based on result-oriented Monte Carlo simulation, and the spatial and velocity relationship of an aircraft pair after an encounter period is needed. We designed a scenario construction model to characterize the spatial and velocity of an aircraft pair, where the encounter period is fixed and set to 25 s according to the warning

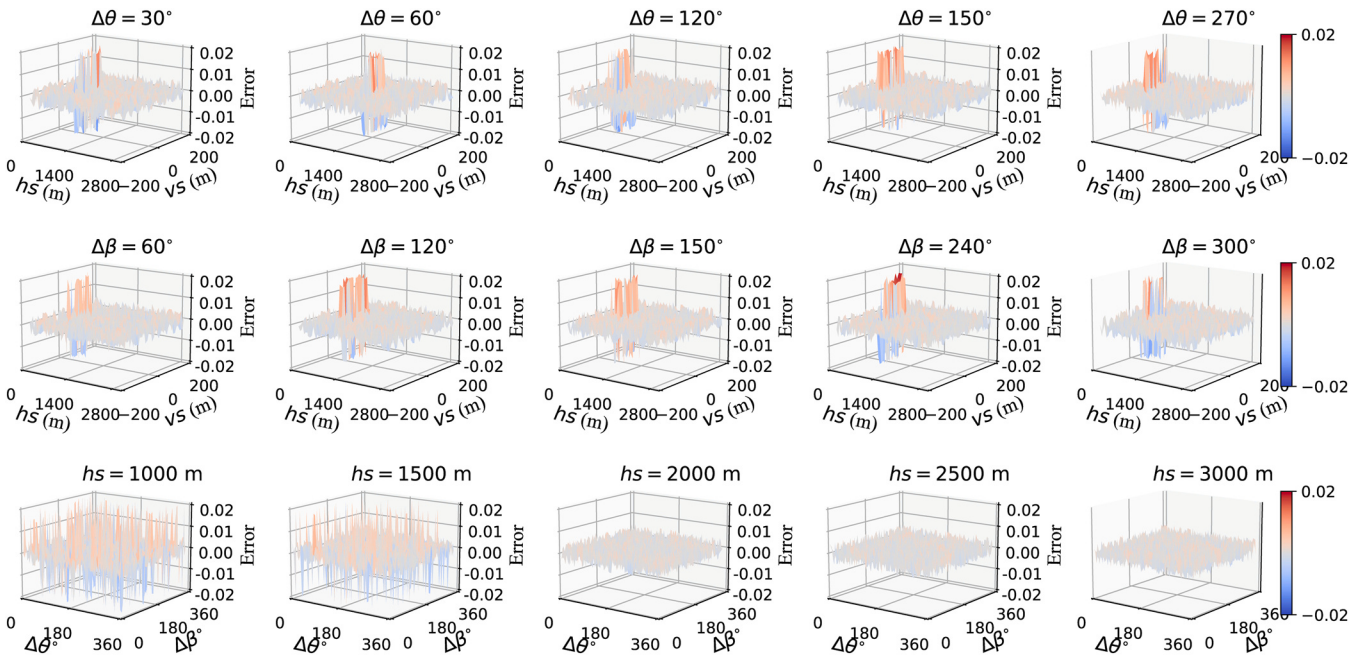


Fig. 16. Comparison of strategic failure probability and result-oriented Monte Carlo simulation results.

mechanism mentioned in Section 2.1. The input of the scenario consists of four variables, angle between the velocity vectors of the two aircraft ($\triangle\theta$), horizontal separation (hs), vertical separation (vs) and azimuth ($\triangle\beta$), as shown in Eq. (31):

$$X = [\triangle\theta, \triangle\beta, hs, vs] \tag{31}$$

The output of the scenario includes the position, the headings of the two aircraft, and the extended collision zone, as shown in Eq. (32):

$$Y = \left[p_i, p_j, \theta_i, \theta_j, l_{cz}, w_{cz}\right] \tag{32}$$

where subscripts i and j designate the two aircraft, p is the position of aircraft, θ is the velocity direction, and l_{cz} and w_{cz} represent the length and width of the collision zone. The mapping relationship between the input and output variables can be expressed by

$$\begin{cases} p_i = (0,0,0) \\ p_j = (hs{\cdot}\cos\,\Delta\beta, hs{\cdot}\sin\,\Delta\beta, vs) \\ \theta_i = 0 \\ \theta_j = 0 + \Delta\theta \\ \Delta v = \left(v_i{\cdot}\cos\theta_i - v_j{\cdot}\cos\theta_j, v_i{\cdot}\sin\theta_i - v_j{\cdot}\sin\theta_j, 0\right) \\ l_{cz} = t_{\text{warning}}\ {\cdot}\|\Delta v\| \\ w_{cz} = 2{\cdot}L_{en} \end{cases} \tag{33}$$

where v_i and v_j are the velocities of aircraft, the values can be obtained from Table 3, t_{warning} is the encounter period, which is defined as 25 s.

The input variables X are the combination of velocity, azimuth, horizontal separation, and vertical separation. For each scenario, the position and velocity relationships of an aircraft pair are determined. Due to random errors, the trajectory points fluctuate around the original path, following a normal distribution with parameters shown in Table 4. A total of 1×10^8 experiments are conducted to generate these trajectory points. By counting how many fall into the extended collision zone, we obtain the Monte Carlo simulation result. The scenario model captures all spatial state combinations of the aircraft pair using four meaningful variables, simplifying the Monte Carlo input, improving computational efficiency, and facilitating the analysis of results. Fig. 14 illustrates the construction process of the result-oriented Monte Carlo experiment with several examples.

4.2.2. Result analysis

Before using Monte Carlo simulation to validate the strategic mitigation failure model, it is essential to demonstrate its effectiveness. A key criterion for this validation is the convergence of probability values over a large number of iterations. If the probability stabilizes as the number of simulations increases, the Monte Carlo results can be considered reliable. As shown in Fig. 15, 2000 simulations are conducted across three typical scenarios. In these cases, the probability values gradually converged to fixed intervals as the number of iterations increased. This confirms the effectiveness of Monte Carlo simulation, the assessed results from proposed models can be validated by comparing the simulation results.

Fig. 16 shows several samplings of the comparisons between the simulation result and the assessed conflict probability, which characterizes the error between two results in the case of variable angles between the velocity vectors of aircraft, azimuths, vertical separations, and horizontal separations, where the encounter period is 25 s. Each subplot corresponds to the different spatial and velocity relationships of the aircraft pair, and a series of comparisons show that the assessed probabilities match well with the simulation results. Specifically, the largest magnitude of the error for all cases shown is 2.1%. For the mean error, the contrast is even more pronounced, with all errors remaining well below 1% in magnitude, and many of them are approximately 0.05%. Considering the practical application requirements, this result is more than adequate.

In addition, it is interesting to note that when the intruder is located at the edge of the extended collision zone, the assessment error is on the high side, which can be explained by the fact that this edge happens to be close to the mean of the intruder's position distribution, resulting in very different results (conflict or not) for small fluctuations, and therefore a larger error in the assessment.

In order to further understand the effect of parameters in the proposed model, the conflict probability under various angles between the velocity vectors of the two aircraft, azimuths, horizontal separations, and vertical separations are analyzed respectively. As shown in Fig. 17, the velocity angle difference between an aircraft pair determines the relative velocity, and when the azimuth is located in a certain range in the opposite direction of the relative velocity, the conflict probability is

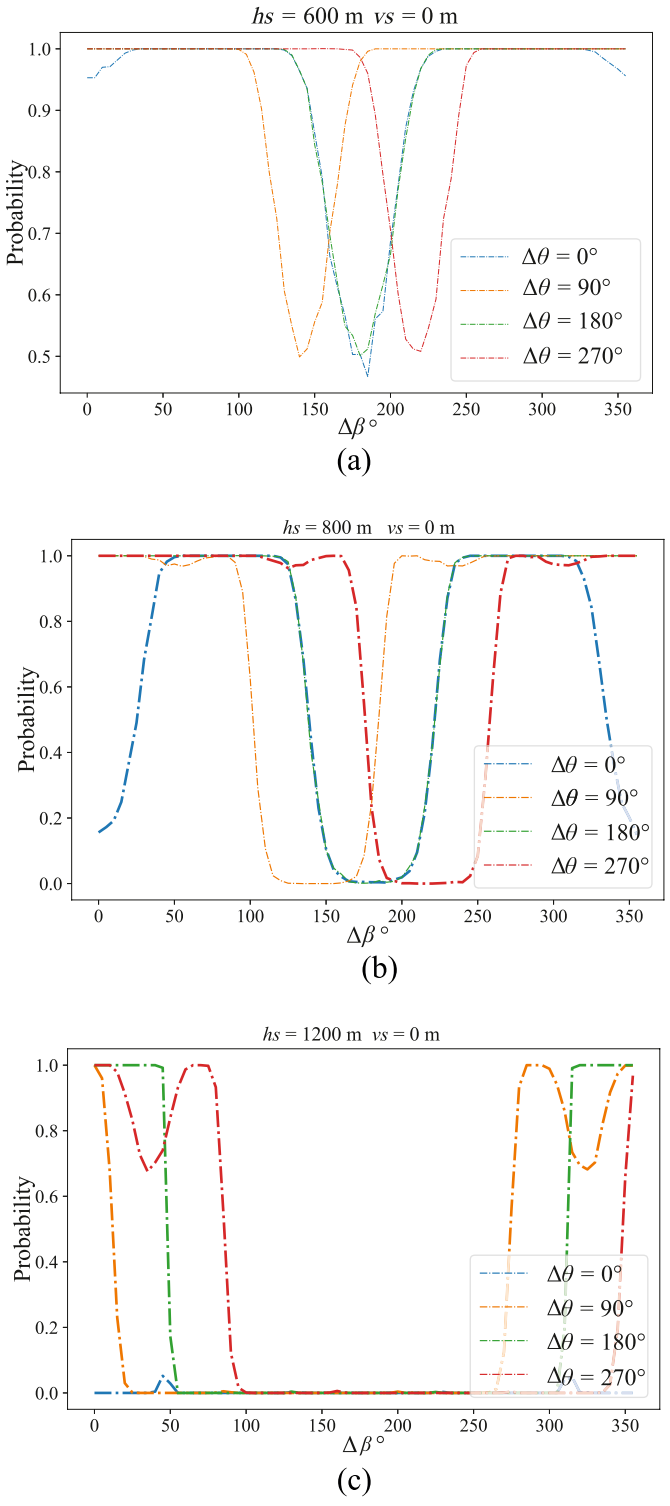


Fig. 17. Effect of relative velocity angle and azimuth on the strategic mitigation faliure.

minimized (or even 0), and this range is obvious with the increase of the horizontal separation. For example, when the horizontal separation is 1200 m, the azimuth range with the probability of 0 is obviously larger than the corresponding case of 600 and 800 m. In addition, the relative velocity of an aircraft pair determines the scope of extended collision zone, so even at the same azimuth, the probabilities corresponding to different relative velocity directions are distinctive.

Fig. 18 shows the effect of horizontal and vertical separation on conflict probability, which is plotted as a function of the encounter period. The first subplot takes the horizontal separation as a parameter, with the velocity angle difference set to 90°, azimuth at 0°, and vertical separation fixed at 0 m. For short encounter periods, the covariances are small and the conflict probabilities are a strong function of horizontal separation. For larger encounter periods, the covariances expand, and the conflict probability becomes a weaker function of the horizontal separation. A horizontal separation of 1200 m can be viewed as a threshold. For horizontal separations less than 1200 m, the probability of conflict decreases as the encounter period increases. Beyond this threshold, the probability of conflict initially increases and then decreases as the encounter period extends, eventually converging and gradually approaching zero. The second subplot illustrates the effect of vertical separation. As vertical separation increases, the conflict probability decreases, showing an approximately inverse relationship with the encounter period due to the growth of covariance. This trend parallels the behavior observed in the first subplot when the horizontal separation is set to 0 m.

4.3. Process-oriented simulation for validating tactical mitigation failure

4.3.1. Simulation setup

The validation of the tactical mitigation failure model is based on process-oriented Monte Carlo simulation, which means that the flight process needs to be modeled, involving latency parameters and sensor errors. In the simulation, the ownship is positioned at the origin of the coordinate system with a velocity angle of 0. Due to various latency factors, there will be a lag in the execution of the avoidance maneuver. The ownship will move toward the intruder with initial relative velocity in this process, but the trajectory may be different in each simulation due to the compass heading error and compass pitch error. The intruder remains relatively stationary throughout the process, with the collision zone defined as the superposition of the collision envelope (refer to Eq. (6)) and the shortest maneuver distance (see Eqs. (18), (20), and (22)) assigned to it. The ownship initiates maneuver once the latency time has elapsed. However, if its position falls within the conflict zone at that moment, avoiding LOWC becomes impossible, indicating a failure in tactical conflict mitigation.

Based on the above analysis, we design a scenario construction model to characterize the relative flight trajectory during encounter. The input consists of six variables: relative velocity direction ($\triangle\theta$), azimuth ($\triangle\beta$), horizontal separation (hs), vertical separation (vs), heading error (ω_h), and pitch error (ω_p), as shown in Eq. (34):

$$X = \left[\triangle\theta, \triangle\beta, hs, vs, \omega_h, \omega_p\right] \tag{34}$$

To enhance the simulation effect, the relative velocity direction must be within a specific range to ensure a potential risk between the aircraft pair. The interval is determined by Eq. (23), and within this range, the relative velocity direction follows a uniform distribution, expressed as $\triangle\theta \sim U(\theta_{\min}, \theta_{\max})$. The position of the intruder can be expressed as $p_j = (hs \cdot \cos\Delta\beta, hs \cdot \sin\Delta\beta, vs)$. The output is the final relative position of the ownship after latency time p_i^t, the mapping relationship can be expressed as

$$p_i^t = p_i + \sum_{i=1}^{t} \Delta v\left(\cos\omega_p^i \cdot \cos\left(\Delta\theta + \omega_h^i\right), \cos\omega_p^i \cdot \sin\left(\Delta\theta + \omega_h^i\right), \sin\omega_p^i\right) \tag{35}$$

where $p_i = (0, 0, 0)$ represents the initial position of ownship, t denotes the latency time, and Δv and $\Delta\theta$ are the relative velocity and direction. Eq. (35) divides the latency time into t periods with a time span of 1 s. Within each period i, the heading error ω_h^i and pitch errors ω_p^i are randomly generated. The cumulative displacement over all time periods determines the final position of the aircraft.

Fig. 19 presents the construction of a process-oriented Monte Carlo simulation, accompanied by several illustrative examples. Specifically,

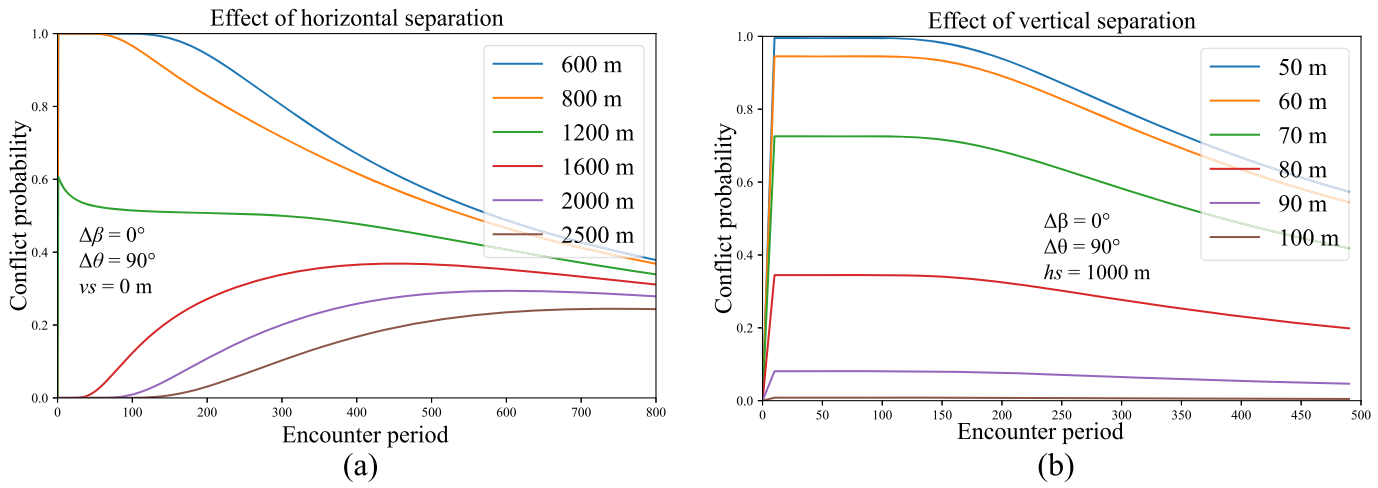


Fig. 18. Effect of horizontal and vertical separation on the strategic mitigation faliure.

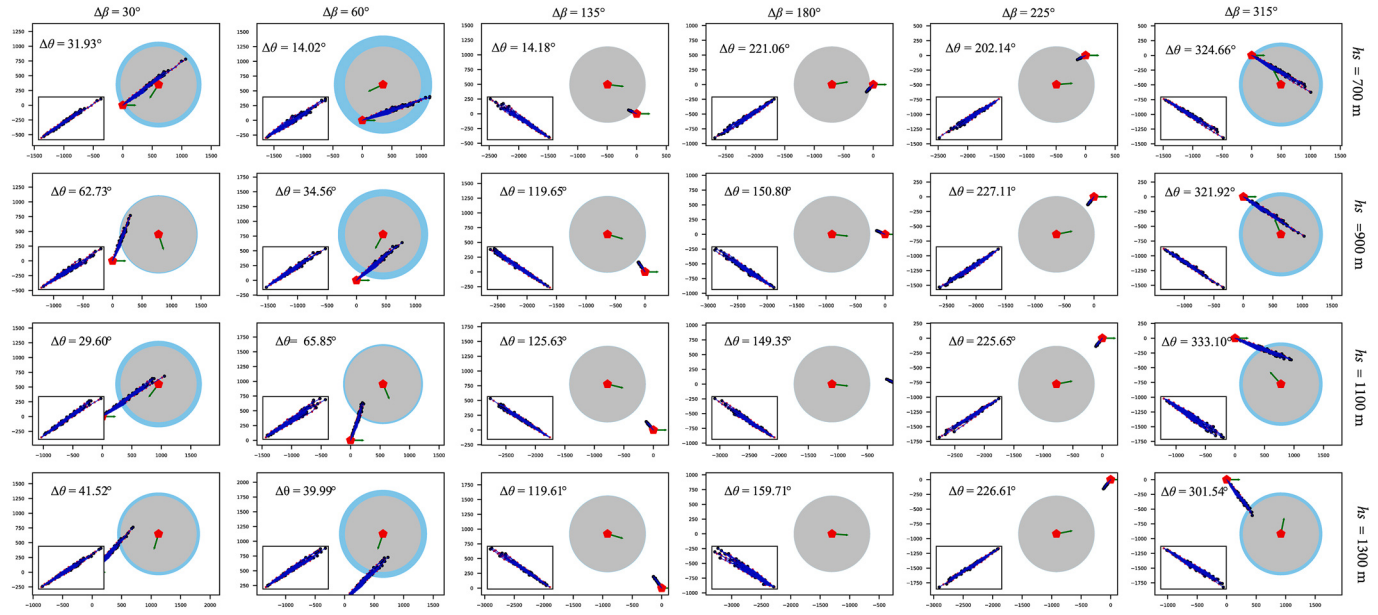


Fig. 19. Process-oriented Monte Carlo experiment with vertical separation of 0 m.

for the initial relative positions of the two aircraft, 1×10^8 random experiment is conducted to generate a corresponding number of trajectories. These trajectories vary based on latency time and error, with each resulting in a distinct final position. The Monte Carlo simulation result is obtained by calculating the ratio of the number of final positions that fall within the minimum maneuvering area to the total number of experiments.

4.3.2. *Result analysis*

Based on the description in Section 4.2.2, we also selected several representative scenarios to validate the effectiveness of the process-oriented Monte Carlo simulation. As shown in Fig. 20, the results show that after a certain number of iterations, the probability values tend to converge, indicating the effectiveness of this simulation.

Monte Carlo simulations are performed with different relative velocity directions, azimuths, horizontal separations, and vertical separations. Fig. 21 shows the failure probabilities as a function of horizontal separations, which are generated by the tactical mitigation failure model and Monte Carlo simulation, respectively. The results demonstrate a strong congruence between the probabilities generated by our model and the simulation results, with an average error margin of just 1. 4%. Notably, the majority of these errors are significantly less than 1% in magnitude, underscoring the model's precision. By analyzing these numerical examples, the conflict probability is directly related to the horizontal separation, the higher this separation, the greater the probability of tactical mitigation failure in the same condition. Meanwhile, if the difference between the azimuth and the relative velocity angles is smaller, the calculated failure probability will increase.

In addition, we found that Monte Carlo empirical results are slightly higher than the assessed probability in some combinations of parameters. The cumulative effect of errors may explain this bias: In Monte Carlo simulations, we directly superimpose the wind error into the final position of UAS, and do not consider the cumulative effect in the flight process like the pitch error and the heading error. This simplification increases the likelihood of LOWC cases in the simulation, particularly at longer horizontal distances. Such cumulative errors may cause the intruder to avoid the collision envelope, and neglecting these effects may result in higher simulation values.

Three maneuvers are incorporated into tactical mitigation: heading adjustment, altitude adjustment, and speed adjustment. To evaluate the

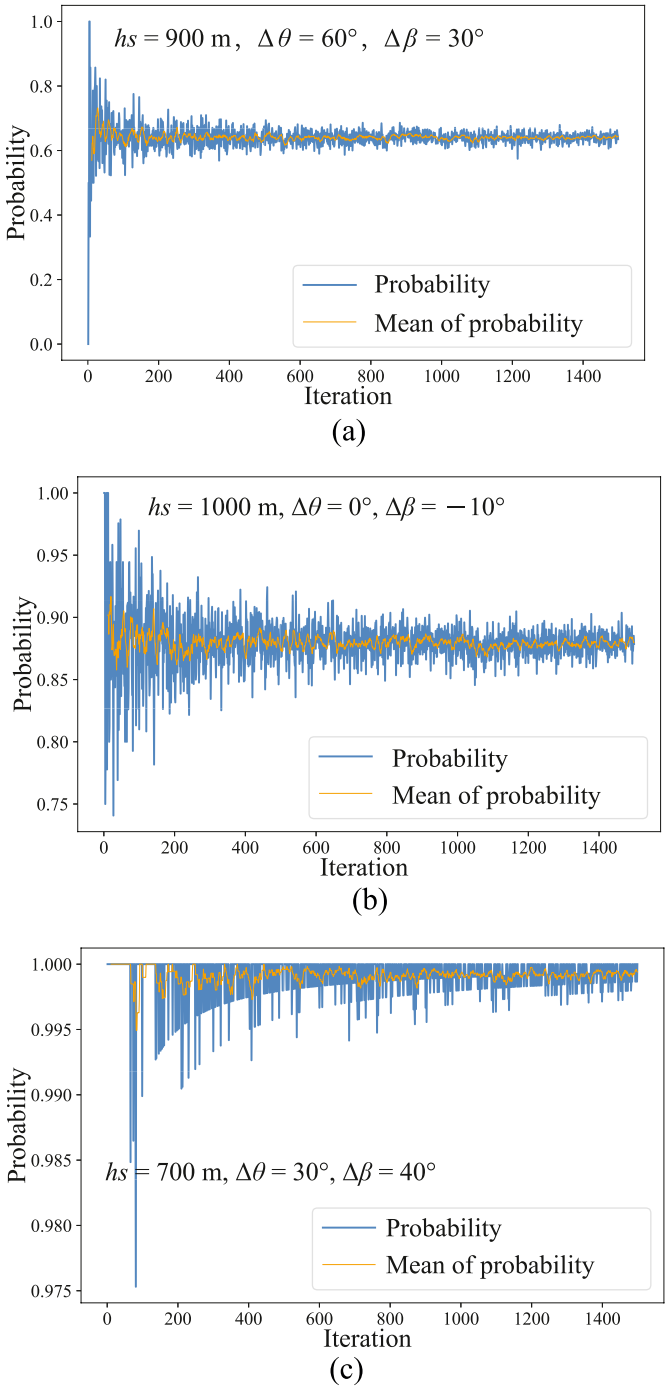


Fig. 20. Relationship between the probability calculated by process-oriented Monte Carlo simulation and the number of iterations.

selection mechanism, two sets of experiments are conducted to analyze how the number of selected maneuvers varies between different vertical separations and maximum speeds, as shown in Fig. 22. In general, the speed adjustment emerges as the most frequently chosen maneuver, indicating its effectiveness in most scenarios. Regarding altitude adjustment, since only the climbing action is considered, it results in the shortest maneuvering distance when the own aircraft is positioned above the intruder and near the edge of the collision envelope. Otherwise, when the vertical separation between the two aircraft is less than 69 m, heading adjustment becomes the preferred choice. For speed adjustment, when the maximum flight speed of the EHang 216 is set to 36 m/s, it requires a greater maneuvering distance compared to the heading adjustment, making the latter the optimal maneuver. However, if the ownship's maximum speed is increased to 41 m/s, the speed adjustment gradually surpasses heading adjustment in effectiveness. Under normal circumstances, the maximum flight speed of the EHang 216 is only about 35 m/s, which means that in most scenarios, speed adjustment is less effective than heading adjustment.

4.4. Comprehensive simulation for validating the MAC assessment timeline

4.4.1. Simulation setup

This section validates the complete MAC risk assessment process for the ownship facing cooperative UAS via Monte Carlo simulation, assuming mitigation measures operate independently during the MAC assessment. Following the assessment framework illustrated in Fig. 1, the timeline primarily involves three measures: strategic mitigation, tactical mitigation, and collision avoidance. The probability of collision avoidance failure is derived from the endogenous risk ratio for DAA systems published by ASTM. This rate represents a conservative risk estimate of NMAC involving DAA-equipped UAS after entering the LOWC volume, based on extensive experimental tests conducted by ASTM. Therefore, the simulations in this section mainly focus on strategic and tactical mitigation. They are made by setting up and simulating numerous airspace scenarios, where the directions of all intruders are randomized, the flight plans are publicly known, and the direction of the ownship is fixed.

Two types of case are constructed based on actual observation and assessment methods to observe the number of incursions into the ownship's DWC volume and to statistically analyze the assessed MAC risk during the ownship's flight. By comparing the incursions number and statistical risk value, the effectiveness of the entire risk assessment timeline proposed in this research is validated. A total of 14 different density points, configured by the number of aircraft in the area of interest ($N_v = 4, 9, 16, 25, 30, 36, 42, 49, 56, 64, 72, 81, 90, 100$) are tested in a series of simulations with at least samples $N_{mc} = 5 \times 10^4$. For every simulation, the area of interest is maintained at 100 km^2. Fig. 23 illustrates two simulation samples with 25 and 100 aircraft. By adjusting the flight plan, the number of intruders in conflict with the ownship is restricted to at most one at any given time step. Each aircraft is represented by a point with an arrow depicting its velocity vector. In all samples, the flight plan of the ownship is fixed, following the diagonal of the area, and all aircraft are set at the same altitude. Each of the simulations are run for a range of time that is needed for the ownship ($V = 25$ m/s) to cross the area. The time-step, on the other hand, is fixed at 1 s.

For the case of actual observation, at each time step, the relative position and velocity between each intruder and the ownship are obtained. The aircraft positions are perturbed on the basis of the environmental error parameters shown in Table 4 to determine whether the intruder enters the extension conflict zero of the ownership, causing a strategic conflict and triggering tactical conflict mitigation. Since strategic and tactical mitigations are assumed to be independent, tactical mitigation is still initiated based on the relative positions and velocities of the two aircraft as defined in the flight plan, without considering position deviations caused by errors. The minimum maneuver distance is calculated according to the three maneuvers described in Section 3.2.2 and the maximum approach time is then compared with the latency time derived from the latency parameters in Table 5. If the latter is greater, it indicates a tactical mitigation failure, which means that the intruder has entered the DWC volume of the ownship. Such an event is counted as a collision, after which the intruder is removed from the simulations. The main output parameter is the expected value of LOWC observation, which is derived from the recorded occurrences of LOWC during the entire Monte Carlo set of airspace samples, $j = 1, 2, \ldots, N_{mc}$. The expected value of LOWC observation is presented in Eq. (36):

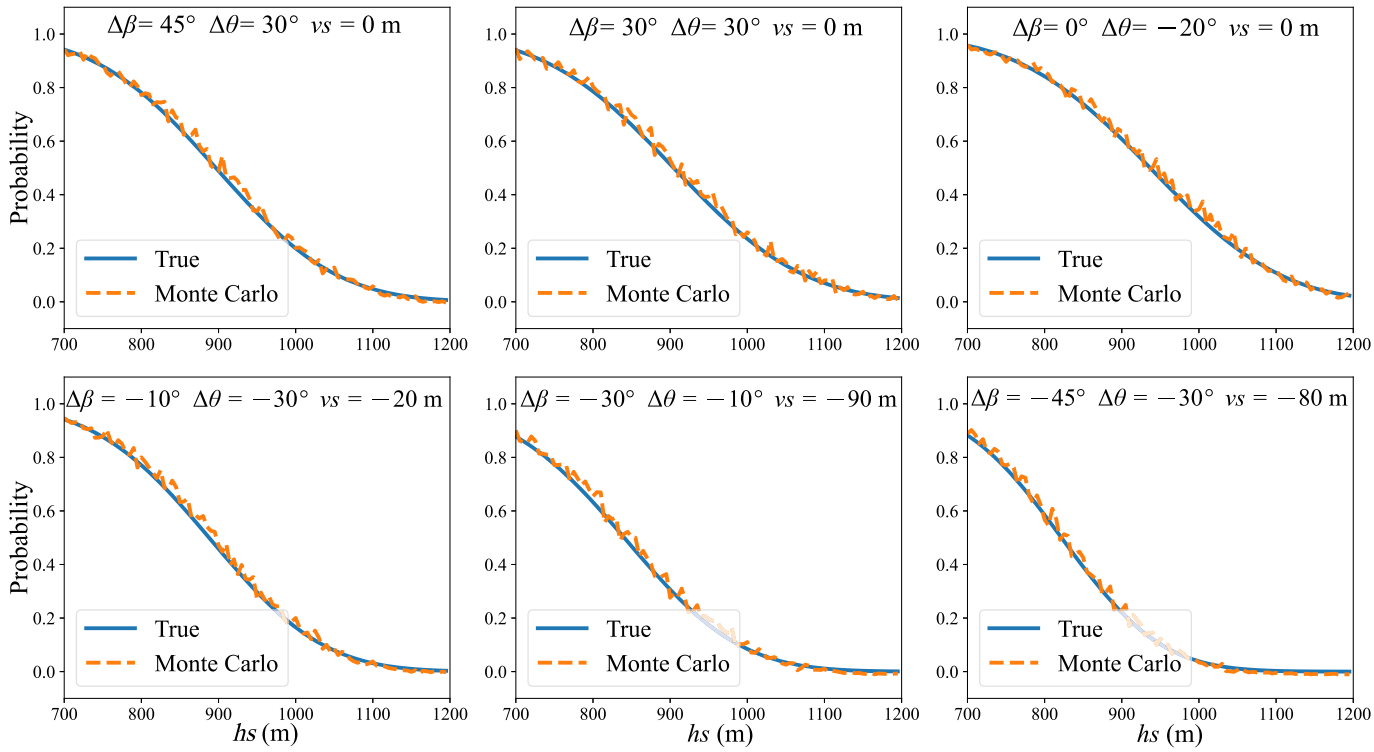


Fig. 21. Comparison of tactical failure probability and process-oriented Monte Carlo simulation results.

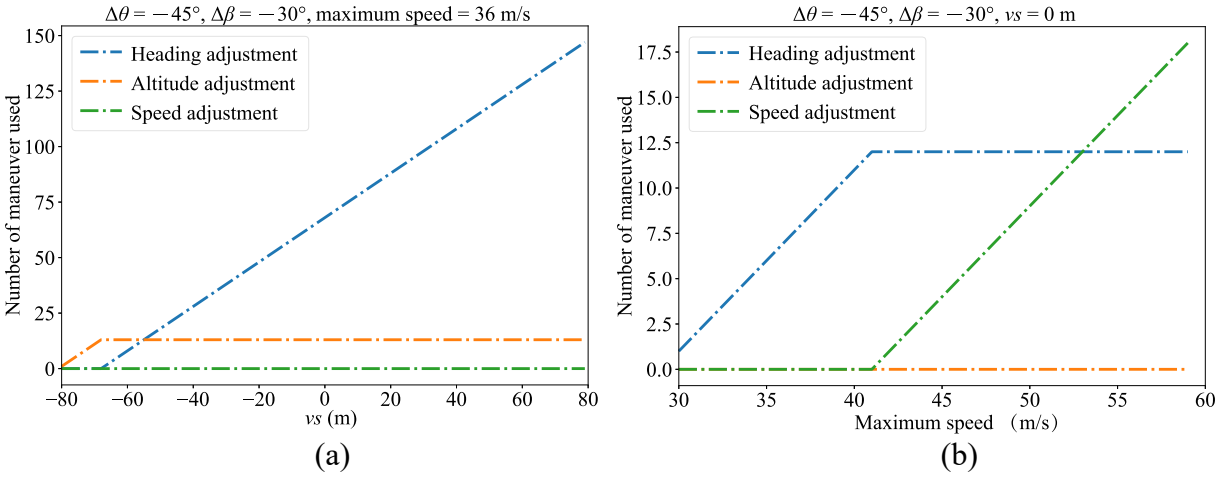


Fig. 22. Frequency of maneuver usage during the tactical phase.

$$E[N_{\text{lowc}}] = \frac{1}{N_{\text{mc}}} \sum_{j=1}^{N_{\text{mc}}} N_{\text{lowc}}^{j} \tag{36}$$

where N_{mc} is the number of airspace samples and N_{lowc}^{j} is the number of observed LOWCs in sample j.

For the case of assessment methods, at each time step, the probability of strategic mitigation failure is calculated based on the model described in Section 3.2.1, a nonzero value indicates the risk of strategic failure. Next, using the positional and velocity relationship between the intruder and the ownship at that time step, the probability of tactical mitigation failure is calculated according to the model in Section 3.2.2. The product of these two probabilities represents the LOWC value of the ownship at that time step. The LOWC risk in a sample is the sum of the risks corresponding to all time steps. The main output parameter is the expected value of the LOWC assessment, which is derived from the recorded LOWC values $R_{\text{lowc}}^{j,i}$ of time step i in airspace samples, $j = 1, 2, \ldots, N_{\text{mc}}$, as shown in Eq. (37):

$$E[R_{\text{lowc}}] = \frac{1}{N_{\text{mc}}} \sum_{j=1}^{N_{\text{mc}}} \sum_{i=1}^{N_t^j} R_{\text{lowc}}^{j,i} \tag{37}$$

where N_t^j is the number of time-step in sample j and $R_{\text{lowc}}^{j,i}$ is the assessed LOWC risk at time-step i in sample j.

In the simulation, the ownship is ensured to encounter at most one intruder in the LOWC condition at any given time step. Therefore, the theoretical maximum value of the LOWC observation at a single time step is 1, which aligns with the range of the LOWC assessment values. Based on this consistency, the relative error between the two can be used

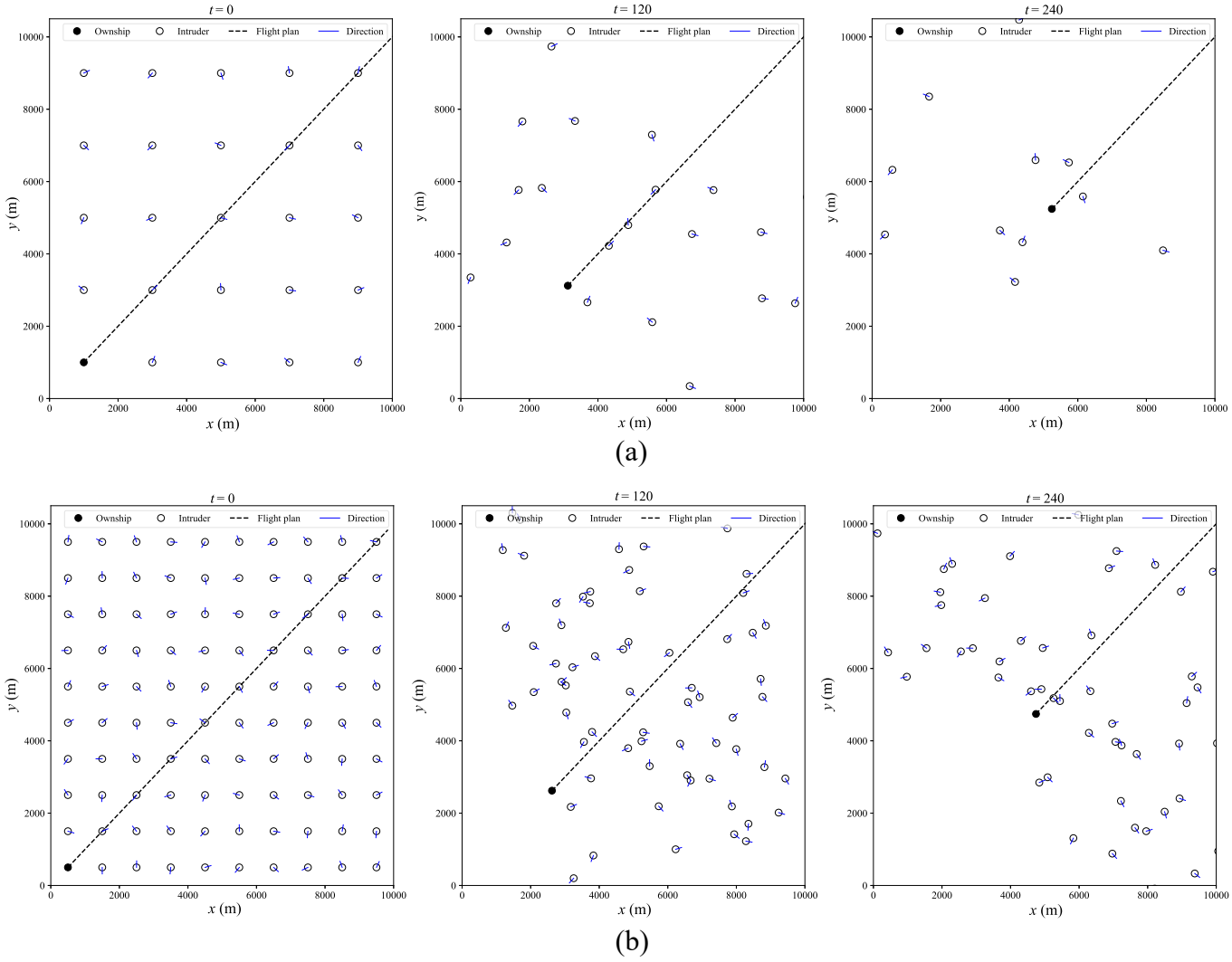


Fig. 23. Comprehensive Monte Carlo experiment with vertical separation of 0 m.

to evaluate the accuracy of the complete MAC assessment method, as shown in Eq. (38):

$$\text{error} = E[N_{\text{lowc}}] - E[R_{\text{lowc}}] \tag{38}$$

4.4.2. Result analysis

This section selects several representative scenarios to validate the effectiveness of the Monte Carlo simulation. The convergence graph in Fig. 24 shows the expected value of LOWC calculated according to Eq. (36), as a function of the number of Monte Carlo simulation runs. The results show that after a certain number of iterations, the probability values tend to converge, indicating the effectiveness of this simulation.

The observation results by Monte Carlo simulation and the assessment results by our models are presented in Fig. 25. Confirming the visual observations, Fig. 25 shows that both parameters increase with airspace density. The expected value of LOWC observation for the ownship in each simulation increases from 0.042, when there are four aircraft in the airspace, to 5.75 when the airspace density reaches 100 aircraft. The curves confirm the reduction of collisions faced by the ownship just by limiting the number of aircraft in the airspace.

The observed values, represented by the blue dashed line, and the assessed values, shown by the red solid line, demonstrate a highly consistent trend throughout the entire range. Their differences generally remain within ± 0.07 across all aircraft densities, indicating that the assessment model achieves a strong fit and high assessment accuracy relative to the simulation results, even under the assumption that the mitigation measures in each layer are independent. The error curve remains relatively stable during the low-density phase, but when the traffic density exceeds 56 aircraft, it shows a marked increase before stabilizing at a positive deviation of approximately 0.06. Overall, the error values exhibit an approximately linear growth, aligning with the anticipated significant increase in LOWC risk as traffic density rises. Additionally, it is notable that in most cases, the observed LOWC values are higher than the assessed ones. This phenomenon may be attributed primarily to two factors: (1) Although the scenario limits the ownship to face at most one intruder per time step, occasional positional uncertainties can lead to multiple aircraft simultaneously entering the LOWC. This chain-trigger effect consistently causes the observed values to be higher than the assessed values. (2) In the simulation, local aircraft densities may surpass the global average, increasing the likelihood that intruders are too close to the ownship to effectively execute tactical mitigation measure. This localized density concentration becomes particularly pronounced at higher airspace densities, explaining why the positive deviation tends to stabilize.

4.5. Sensitivity analysis

The Monte Carlo simulations above have validated the accuracy of the key models and the reliability of the entire assessment timeline. In this section, we construct a general scenario to analyze how critical

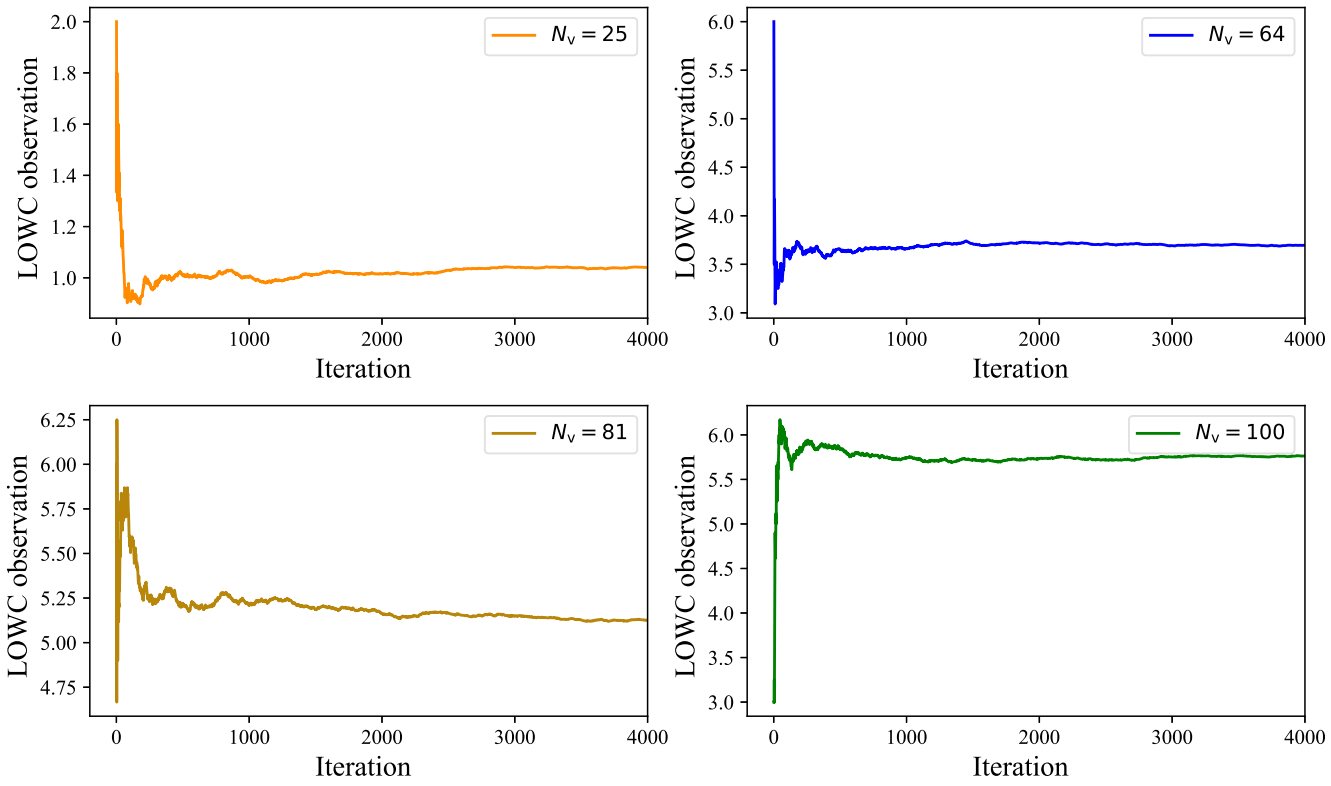


Fig. 24. Relationship between the expected value of LOWCs observed by Monte Carlo simulation and the number of iterations.

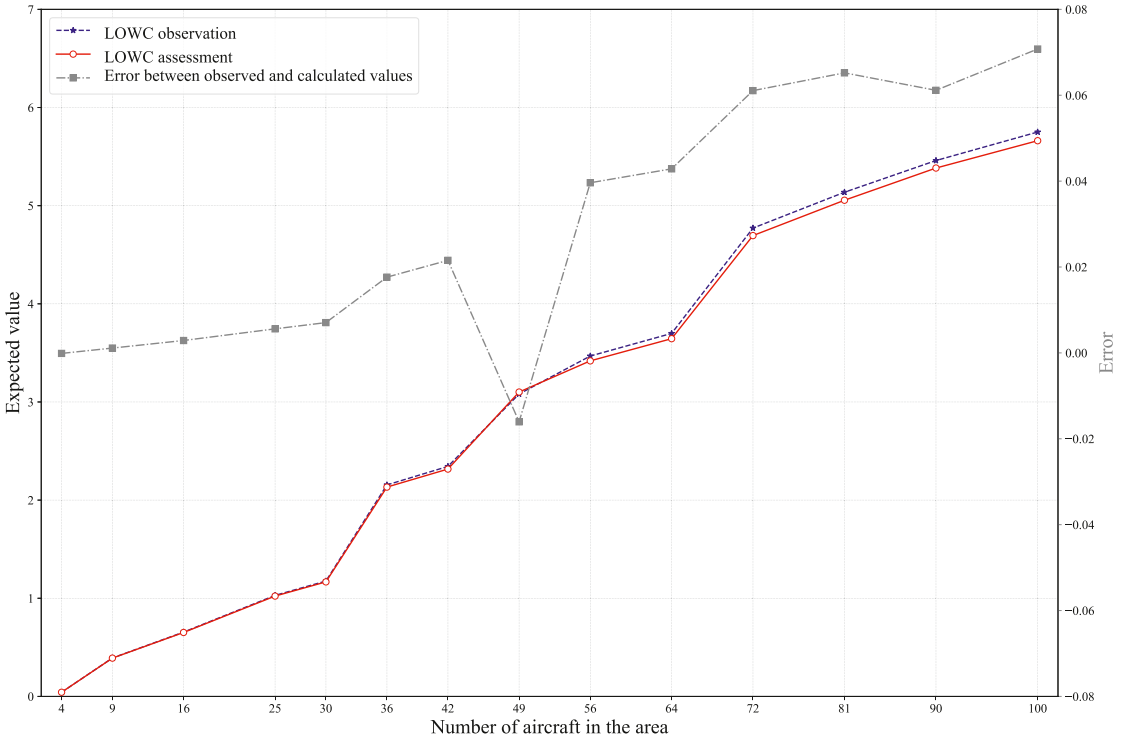


Fig. 25. Expected values of LOWC observation and LOWC assessment, and their difference in relation to the number of intruder.

parameters in Section 4.1 affect the assessment results. In the scenario, the intruder has a relative bearing of 45°, the ownship's heading is set to 0°, and the intruder's heading is 280°, with the other performance parameters consistent with those of Table 3. The distance between the two aircraft is set between 1000 and 2000 m. We vary the range of DWC volume, the environmental parameters influencing position error (listed in Table 4), and the latency parameters influencing maneuver response (listed in Table 5). Then compare the MAC probabilities to analyze their

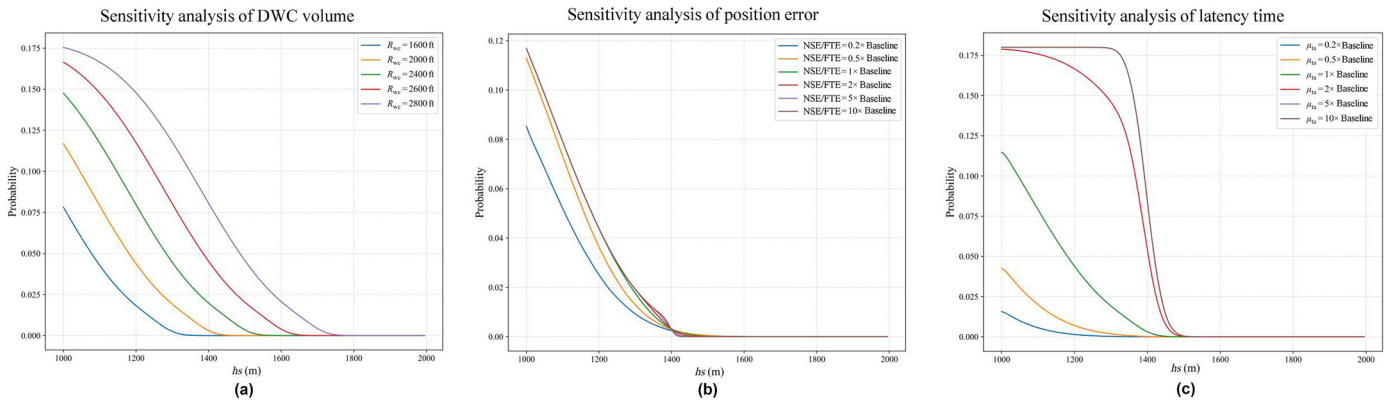


Fig. 26. MAC risk comparison curves calculated under varying values of the DWC volume, position error, and latency time.

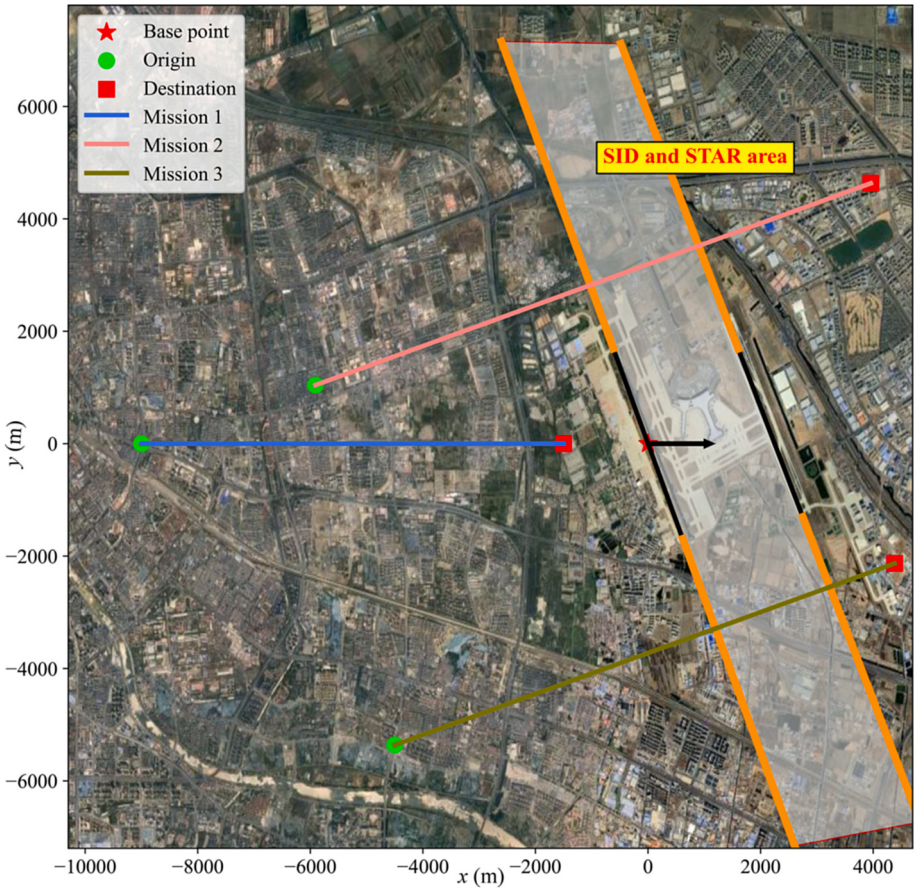


Fig. 27. Typical real-world scenario designed for the study.

Table 6
Specification of flight plans for missions.

Information	β (°)	Origin hs (m)	vs (m)	θ (°)	Flight time (s)	Flight speed (m/s)
Mission 1	180	9,000	100	0	500	15
Mission 2	170	6,000	70	20	700	15
Mission 3	230	7,000	100	20	630	15

influence on the final results.

Fig. 26 illustrates the MAC probability under the influence of the DWC volume range, position errors and latency time. The data show that MAC probability is highly sensitive to the DWC volume. A larger DWC volume significantly raises the entire risk curve and shifts the inflection point of risk reduction toward greater horizontal separations, indicating that a relatively high risk level still exists even at increased distances. This implies more stringent safety requirements for such DWC values, while unavoidably leading to a reduction in airspace capacity. For investigating the impact of position errors on MAC risk, the environmental parameters listed in Table 4 were proportionally scaled. The results indicate that the sensitivity to position errors is relatively low, with influence mainly concentrated at smaller separations. Within the positional relationship of aircraft defined in this scenario, increasing position errors leads to a higher MAC risk. This is because larger errors increase the likelihood that the intruder enters the extended conflict zone, increasing the failure probability of strategic mitigation. As

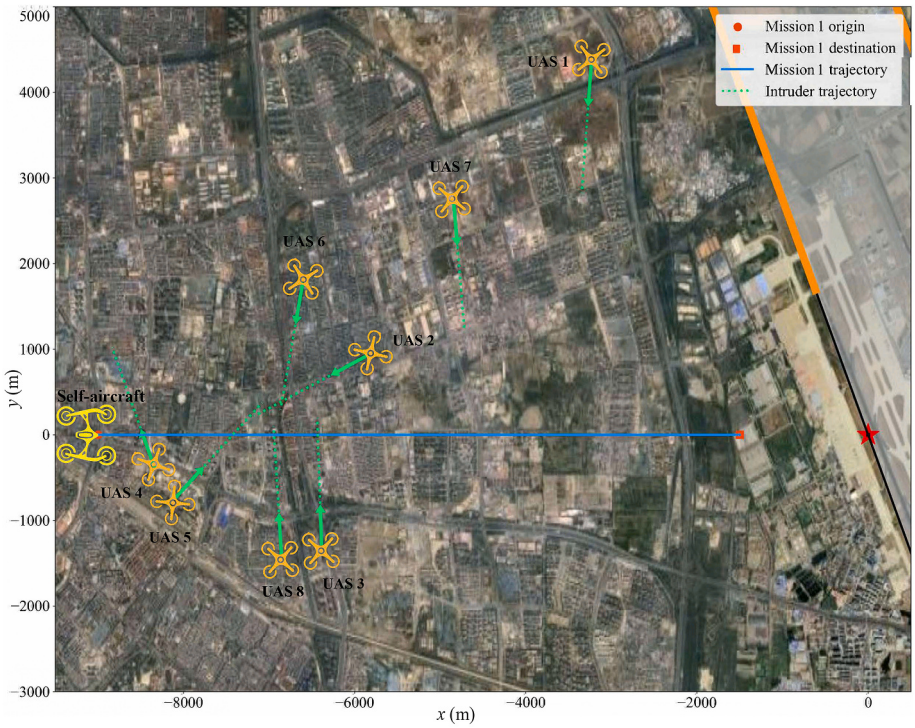


Fig. 28. Cooperative UAS high density operation.

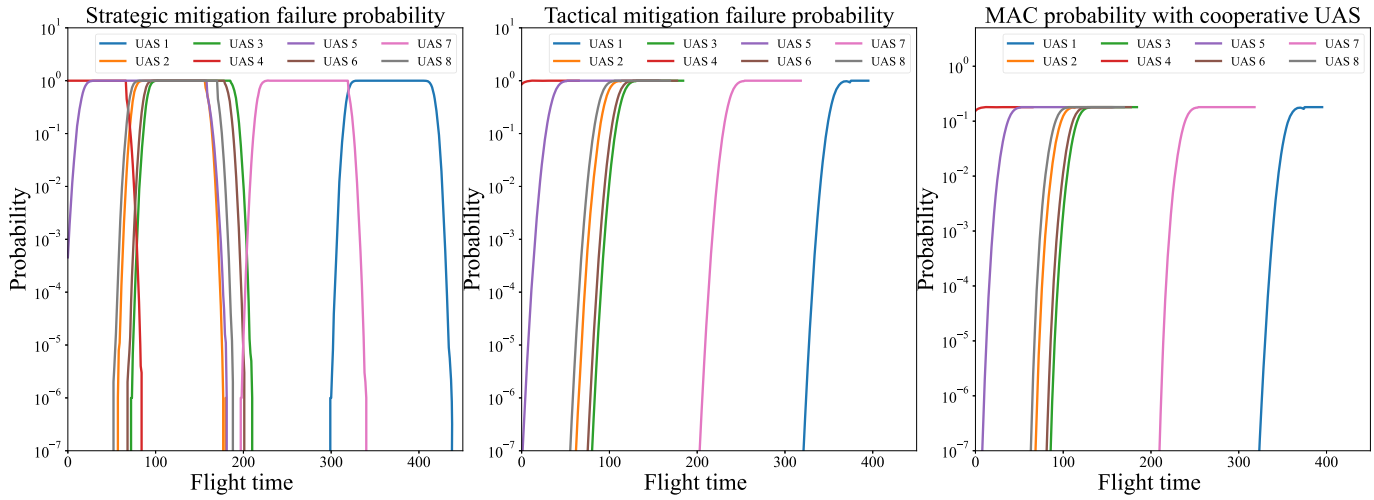


Fig. 29. Mitigation failure probability with cooperative UAS at each phase.

separation increases, the influence of position errors decreases, leading the risk curves for different error levels to converge. However, in dense airspace operations, attention should still be paid to the amplifying effect of positional inaccuracy on the short-range conflict. The relationship between the latency time parameters listed in Table 5 and MAC probabilities was examined in a similar manner by proportionally scaling the parameters. The latency time primarily affects the failure probability of tactical mitigation. Longer latency reduces the maneuvering distance available for conflict avoidance, thereby increasing MAC risk. The curve trends also reflect this characteristic. In particular, increased latency substantially delays the risk decay process and greatly amplifies MAC probabilities in low separations. A non-negligible level of risk remains even at larger separations in extreme cases. In summary, DWC volume and latency time exhibit high sensitivity to MAC risk and should be prioritized in risk control and parameter selection, while position error mainly impacts scenarios with low separation distances.

5. Illustrative example

This section explains how the proposed MAC probability method can be applied using illustrative examples from a representative real-world environment. The environment includes four representative scenarios: three individual operations of cooperative UAS, non-cooperative UAS, and manned aircraft, as well as their collective integrated operations.

5.1. Real-world environment description

A typical urban area (16 km × 16 km) is selected, including the airport SID and STAR area. The ownship in this environment is selected as the EHang 216, and the intruder is DJI Mavic 3. The basic flight

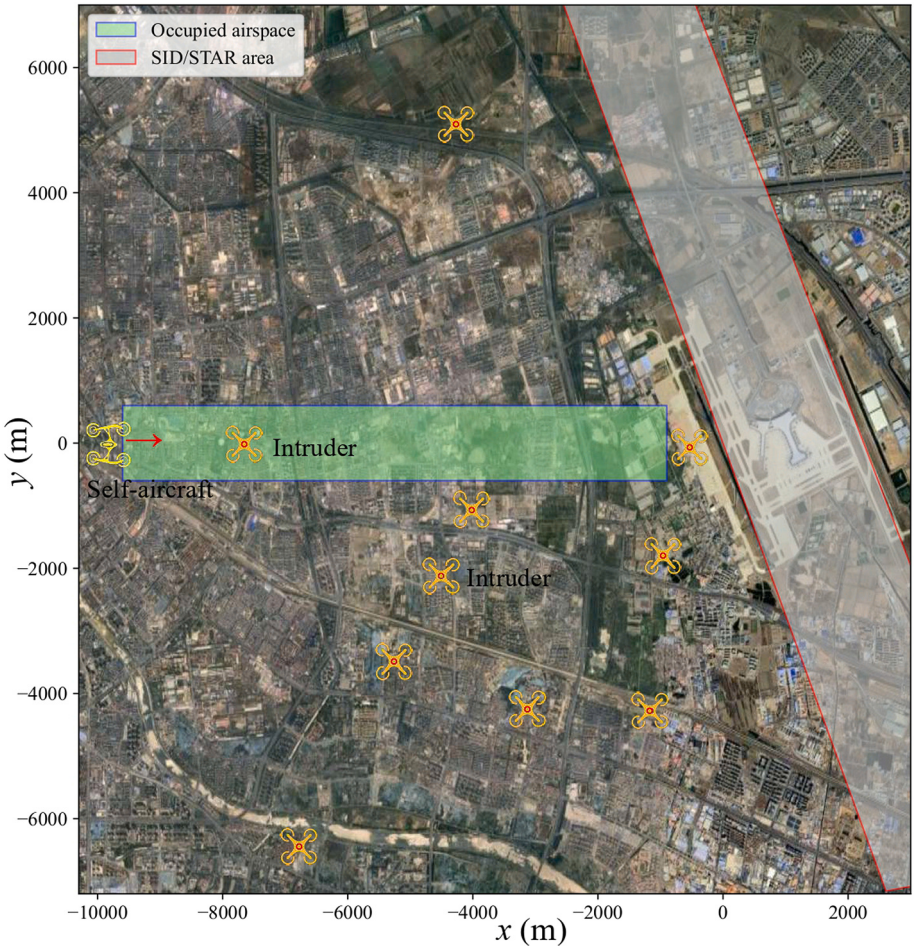


Fig. 30. Non-cooperative UAS intrusion scenario.

characteristics are shown in Table 3. To ensure realism of the environment, wind impact, NSE, FTE, sensor errors, and response latencies are incorporated into the flight process. The specific parameters for these factors are listed in Tables 3–5.

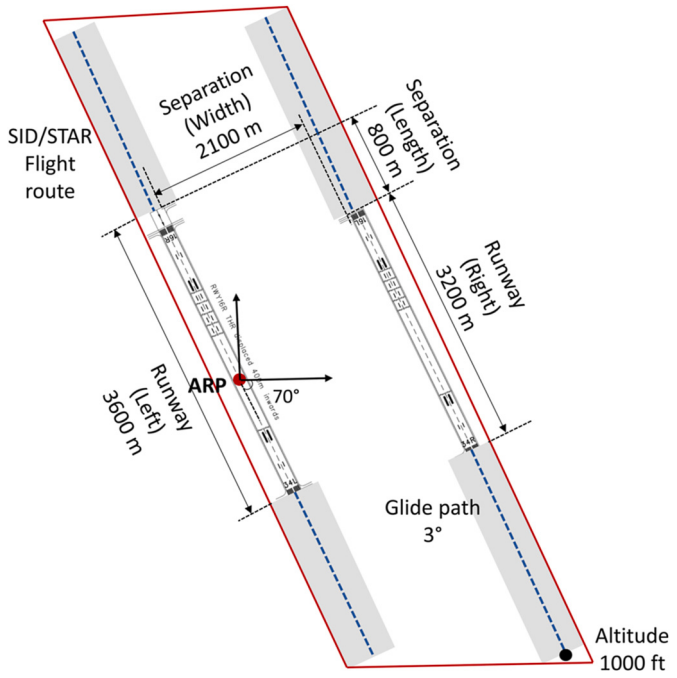


Fig. 31. Diagram of aerodrome alert airspace (top view).

The airport aerodrome reference point (ARP) is considered the reference point for the entire environment, with the east direction as the base reference. The flight information of UAS is characterized by the horizontal separation (hs), azimuth (β), vertical separation relative to the reference point (vs), and velocity direction (θ). The environment for the case study is shown in Fig. 27, where the gray range represents the SID and STAR area, with flights in this area potentially posing a collision risk for manned aircraft.

The ownship requiring MAC probability assessment will carry out three missions, mission one entirely inside the permissible area, mission two with a route through the SID and STAR area, and the last mission spans all areas of this environment and is used to assess the overall MAC probability from all operation types. The flight plans for the missions are shown in Table 6.

5.2. Experimental scenario for each type of operation

5.2.1. Cooperative UAS

To explain the effectiveness of the method in handling future high-density operation, a cooperative UAS simultaneous operational scenario is designed around mission 1, as shown in Fig. 28. This scenario involves eight UAS, with their flight directions indicated by arrows. To visually present the MAC probability assessment results, the spatial positions and velocity directions of these UAS are strategically arranged to create proximity or overlap points with the ownship trajectory in both space and time.

The assessment of P_{cop} takes into account the spatial position of

Table 7
MAC probability with manned aircraft.

Period	0–10 s	10–20 s	21–30 s	31–40 s	41–50 s	51–346 s	347–483 s	484–700 s
P_{PC}^{man}	—	—	0.4130	—	—	—	0.2065	0
$P_{TC\text{-}PC}^{man}$	3.276×10^{-8}	3.455×10^{-5}	4.005×10^{-3}	0.1156	0.5655	1	1	0
P_{man}	1.353×10^{-8}	1.427×10^{-5}	2.063×10^{-3}	4.776×10^{-2}	0.2336	0.4130	0.2065	0

aircraft pairs, the uncertainty in the position, and the information transmission latency, etc. The P_{ST}^{cop} and P_{TC-ST}^{cop} posed by each UAS to the ownship are assessed in chronological order, and these values vary over time, which are shown in Fig. 29. Fig. 29 categorizes risks with a probability below 1×10^{-7} as unlikely and those above 0.99 as inevitable. As the UAS approaches the ownship, both P_{ST}^{cop} and P_{TC-ST}^{cop} gradually increase, reaching a maximum probability of 1 when the UAS enters the ownship's collision envelope. Conversely, when an aircraft pair is moving away from each other, no avoidance maneuvers are necessary, eliminating the risk of tactical mitigation failure. Generally, the failure probability of strategic mitigation at the same time is high than that of tactical phase. This phenomenon becomes more pronounced when UAS are in close proximity, indicating that improving the success rate of strategic mitigation is crucial for ensuring airspace operational safety. Therefore, during the strategic planning stage, the protection volume of UAS should be expanded to achieve more sufficient separation between them.

Combining P_{ST}^{cop}, $P_{TC\text{-}ST}^{cop}$, and $P_{CA\text{-}TC}^{cop}$ obtained from the risk ratio of DAA devices in Section 3.2.3, the real-time MAC probability can be calculated, as shown in Fig. 29. Overall, by assessing the MAC probability of each UAS, the ownship can promptly identify intruders that may pose a remarkable threat and thus take the appropriate collision avoidance measures in advance.

5.2.2. Non-cooperative UAS

According to the dynamic gas model in Section 3.3.1, $P_{non\text{-}cop}$ is mainly related to the mission execution time, the position relationship between ownship and intruders, as well as the intrusion frequency of non-cooperative UAS. Assuming that the non-cooperative UAS will not appear in the aerodrome alert airspace, the mission 1 is used to demonstrate the MAC assessment process with non-cooperative UAS. This paper defines the intrusion frequency of corresponding airspace as 10 times a year. Given the random spatial positioning of intruders in the model, 1000 experimental runs are conducted and the number of intruders at risk in each experiment is counted. Fig. 30 illustrates the location distributions of non-cooperative UAS in one experiment and the positional relationship with occupied airspace swept by ownship. Finally, the MAC probability with non-cooperative UAS during mission 1 is obtained based on Eq. (29) as 1.083×10^{-6}. For the purpose of unifying the assessment unit, this value is defined as. 6.498×10^{-8}/30 s. Since the intrusion frequency varies depending on the range of airspace and the means of control, the assessment result is scalable, which can be obtained based on the specific historical data of different airspace.

5.2.3. Manned aircraft

The scenario focuses on the SID and STAR areas to evaluate the MAC probability between UAS and manned aircraft in Mission 2. The feature of alert airspace is shown in Fig. 31, which is a polygon associated with the precision approach and departure procedure. The structural parameters are related to different runways and their orientations, the angle of glide slope, as well as the UAS altitude limit (set at 1000 ft). Based on airport data, the lengths, directions, and distances between two runways are obtained. The combined collision envelope centered on the ownship, which consists of the collision envelope and the size of the manned aircraft (the radius is 0.56 km and the height is 200 m with reference to Hu et al. (2020)).

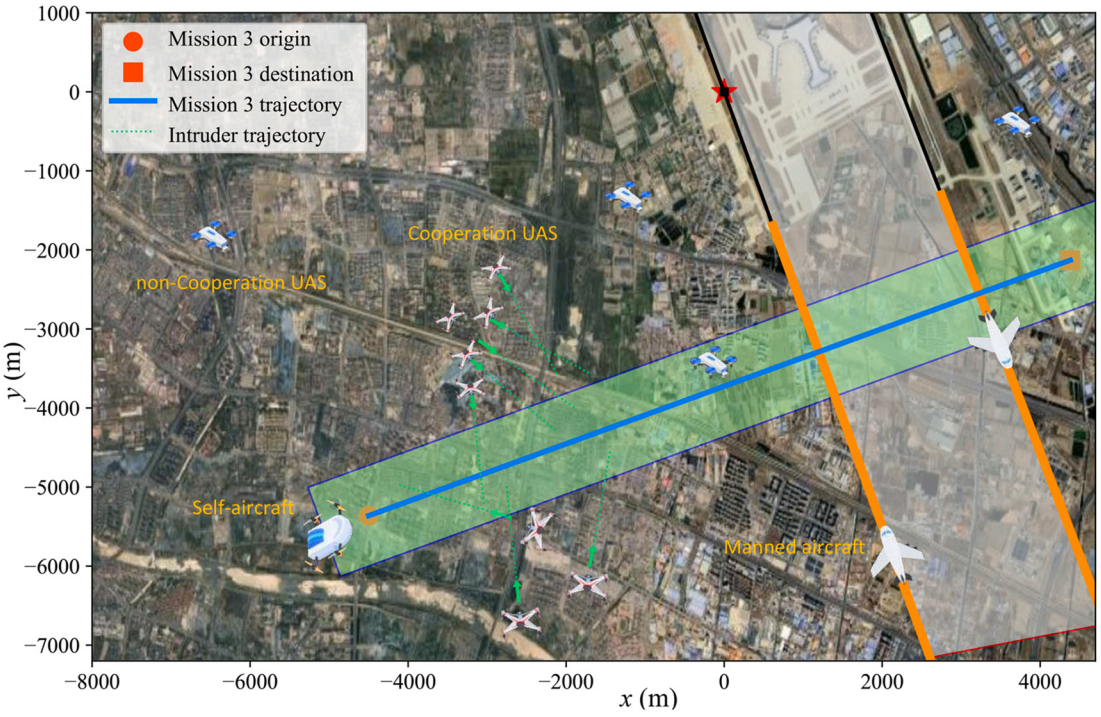
The probability of procedural mitigation failure is affected by the area swept by ownship with a combined collision envelope, as well as the take-off frequency of manned aircraft. In this study, the release interval for a single aircraft is defined as 2 min with reference to the wake turbulence interval standard and the average speed of civil aviation aircraft in the take-off phase. The probability of tactical failure is related to the distance from the SID and STAR area. Table 7 records the MAC probability with manned aircraft during mission 2.

The overlap area of Mission 2's trajectory with the SID and STAR area and the time flying within that area is fixed, and then the release interval of manned aircraft is also a constant, so the procedural mitigation probability remains consistently at 0.413 before entering the SID and STAR areas. At 347 s, the ownship moves away from the first runway, making its collision probability with a manned aircraft dependent solely on the second runway. Consequently, the corresponding collision probability is halved. By 484 s, the ownship has completely exited the SID and STAR areas, eliminating any risk of collision with manned aircraft. To illustrate the tactical mitigation process, the mission is divided into 10-s intervals. Initially, the ownship maintains a high probability of successful tactical mitigation due to its distance from the airport. As the aircraft approaches the SID and STAR areas, the failure probability gradually increases. After 51 s, when the ownship is fully within the area, tactical mitigation is no longer effective, and the MAC probability depends solely on procedural mitigation.

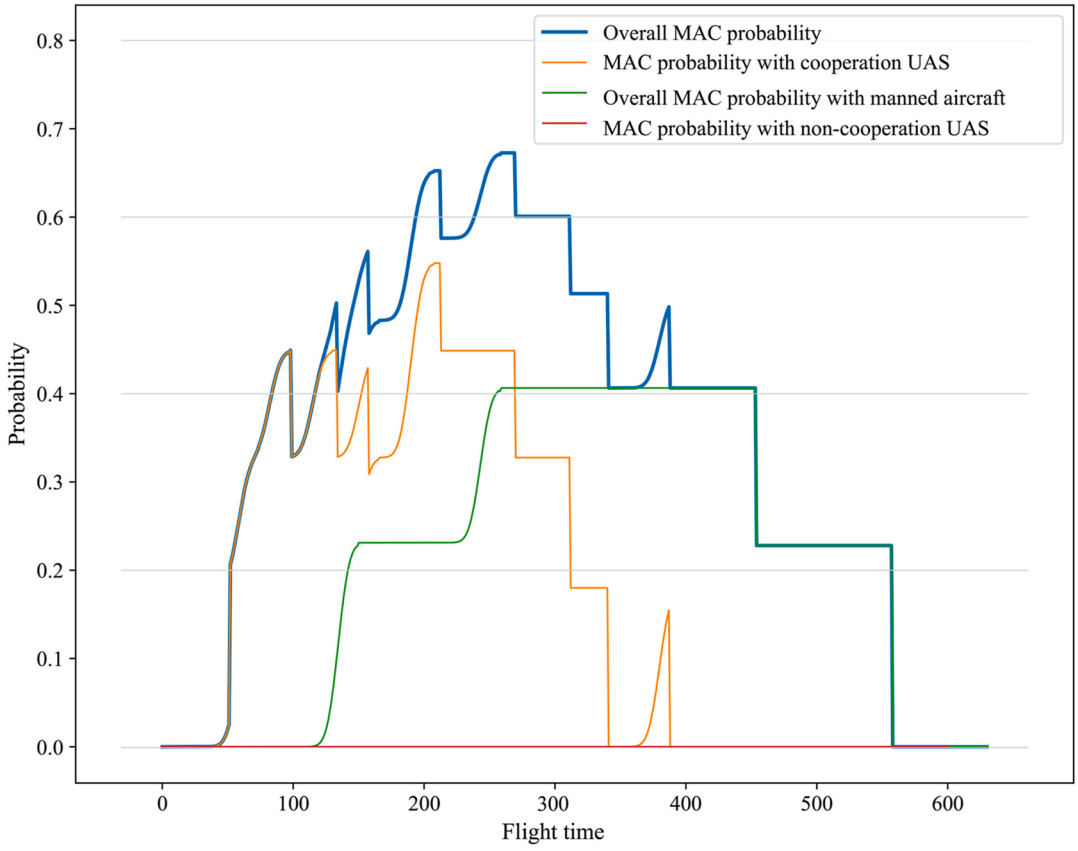
5.3. Experimental scenario for integrated operations

The ownship may face MAC risks from multi-type operations, such as cooperative UAS, non-cooperative UAS, and manned aircraft. This section explains how the overall MAC probability is assessed using all relevant models. Fig. 32 describes a low-altitude integrated operational scenario containing eight cooperative UAS causing conflicts against the ownship with known positions and trajectories, non-cooperative UAS randomly appearing in the course of the ownship's mission with accessible positions and unknown velocities, and manned aircraft flying along a fixed SID and STAR procedure.

The final assessment results are shown in Fig. 32. It can be observed that during the first 100 s of the mission, the overall MAC probability is primarily influenced by cooperative UAS, as the ownship remains relatively far from the SID and STAR area. Between 100 and 400 s, as the ownship approaches this area, the MAC probability associated with manned aircraft becomes increasingly significant, resulting in a surge in the overall MAC probability, especially near 200 s, when cooperative UAS activity intensifies. During this period, multiple trajectories intersect with the ownship's path, leading to a pronounced peak in the MAC probability. After 400 s, the ownship leaves the region of intensive cooperative UAS activity, and the overall MAC probability closely aligns with that of manned aircraft alone. Since the SID and STAR area encompasses two runways, the collision probability with a manned aircraft is reduced by half once the ownship crosses the first runway, which results in a stepped pattern in the probability curve. In general, in this specific integrated operations scenario, the probability of ownship MAC is mainly caused by cooperative UAS and manned aircraft, cooperative UAS having a major role in the intensive activity area, with non-cooperative UAS posing a relatively weak risk of MAC compared to others. This is because this scenario design a future high-density operational demand in which multiple cooperative UAS operate concurrently with the ownship within a confined airspace. Moreover, the MAC risk posed by manned aircraft experiences a sharp increase around 120 s, when the ownship is approximately 4200 m from the SID and STAR area.



(a)



(b)

Fig. 32. Integrated operation scenario with manned aircraft.

This distance may serve as a reference for expanding the protection zone within the airport area.

6. Conclusions and further work

This study presented a method for systematically assessing MAC probability from multi-type operations. Based on the analysis of risk prevention processes for different operations, this method formulated four main barriers to prevent a procedure conflict ending in a MAC and three core timelines to describe the risk evolution. To obtain the overall MAC probability, innovative models were developed for all main barriers, which highlights can be summarized as various external factors, fast-time computation, and multiple maneuver strategies. Monte Carlo simulations show that the probability curves are generally consistent with theoretical calculations. The maximum error in strategic mitigation failure occurs when the intruder is located at the edge of the conflict extension zone, as this condition is more likely to produce unstable simulation data. The simulation probability of tactical mitigation is often higher since the cumulative effects of winds are not considered. However, considering the practical requirements, the accuracy of the results in these models is acceptable for real-world application. The illustrative examples show that the MAC risk posed by the cooperative UAS constitutes the majority of the risks in the scenarios. The use of larger protection volumes in the strategic phase can reduce the whole risk, underscoring the need for SORA to address MAC risks from cooperative UAS in addition to manned aircraft.

There are still some limitations in this research. Firstly, as a newer technology, UAS lack the depth of data available for manned aircraft. As such, the model validation in this study relies on high-fidelity simulations, incorporating diverse environmental and latency data from trusted sources to enhance the credibility of the results. In the future, real flight data from UAS can be used to extract FTE and NSE, enabling further validation of specific components, such as the strategic mitigation failure. Secondly, this study references the alerting logic for small UAS and the DWC volume ranges in the FAA's minimum operational performance standards (MOPSs) to define the assessment parameters, which may not be suitable for all UAS types. Future research should establish assessment criteria for UAS of different speeds and sizes and develop safety separation standards that ensure an equivalent level of safety based on extensive assessment data. Then, this study considers multiple maneuvers, but only a single optimal maneuver is selected for the tactical mitigation execution, without considering combinations of maneuvers. The risk assessment based on multiple maneuver combinations requires further research. Finally, the MAC probability assessment serves as a foundation for risk management in the context of UAM. This assessment must be further extended to incorporate the probability of a fall following a collision, as well as the probability of causing damage to property on the ground or in the air. Together, these components will support the development of a comprehensive air–ground risk assessment model.

Replication and data sharing

The dataset and code used in this research are partially available on request by emailing the corresponding author.

CRediT authorship contribution statement

Jinpeng Zhang: Writing – review & editing, Writing – original draft, Visualization, Validation, Supervision, Software, Methodology, Investigation, Formal analysis, Data curation, Conceptualization. **Yan Xu:** Writing – review & editing, Visualization, Supervision, Resources, Project administration, Methodology, Investigation, Funding acquisition, Formal analysis, Conceptualization. **Kaiquan Cai:** Writing – review & editing, Supervision, Methodology, Formal analysis, Conceptualization. **Victor Gordo:** Writing – review & editing, Supervision, Methodology. **Gokhan Inalhan:** Writing – review & editing, Supervision.

Declaration of competing interest

The authors declare that they have no known competing financial interests or personal relationships that could have appeared to influence the work reported in this paper.

Acknowledgements

This research was partially funded by the National Natural Science Foundation of China (No. 52402395).

Appendix

Incorporating interlayer interactions in assessment framework

The assessment framework is built on the assumption that the mitigation measures operate independently, in line with the officially adopted Swiss-Cheese model. It is undeniable that some scholars remain concerned about the nature of the holes in the cheese and their inter-relationships. As noted by Dekker (2017): The SWM is an important tool in the field of accident analysis and prediction, but unfortunately does not account for the detailed interrelationships among causal factors, which appears to be a challenge. Therefore, we explore the interdependencies between safety layers and enhance the framework to capture the interactions between adjacent mitigation measures.

The discussion of interdependencies extends to both strategic and tactical mitigation, as this combination is the most likely to exhibit mutual interactions. Once strategic mitigation fails, the ownship is responsible for executing a tactical avoidance maneuver upon an intruder, triggered by a warning issued after the strategic failure. In practice, tactical mitigation is partially dependent on the effectiveness of strategic mitigation, which is established prior to flight by designing conflict-free trajectories to avoid spatial and temporal overlaps between aircraft. However, the failure of strategic mitigation often leads to two adverse effects that compromise the performance of subsequent tactical mitigation. First, following the failure of strategic mitigation, the aircraft pair often exhibits small crossing angles and separation distances. This geometric configuration significantly reduces the available temporal and spatial buffers for tactical mitigation. As a result, the time window for maneuvering becomes more constrained, and the options for effective avoidance are limited. More critically, various sources of in-flight uncertainty, such as FTE, NSE, and wind, may cause UAS to deviate from their planned paths, thereby violating strategic separation. Even after strategic mitigation fails, the position uncertainty caused by these errors can lead to a more adverse initial state for tactical mitigation, further increasing the difficulty of effective maneuvering. As environmental complexity increases, such uncertainty-driven failures are becoming a major challenge for tactical effectiveness.

Based on the above, we incorporate the position uncertainty from the strategic phase into the assessment of tactical mitigation, as defined in Eq. (7). Specifically, the combined error covariance of an aircraft pair is assigned to the intruder, modeling it with significant positional uncertainty relative to the ownship. To ensure effective tactical mitigation measure and a conservative assessment, we fit the intruder's position distribution using a 95% confidence interval in both horizontal and vertical directions. The position closest to the ownship within this distribution is then selected as the

actual relative position for tactical decision-making. All subsequent assessment of tactical failure probability are based on this relative position. The graphical explanation shown as follows:

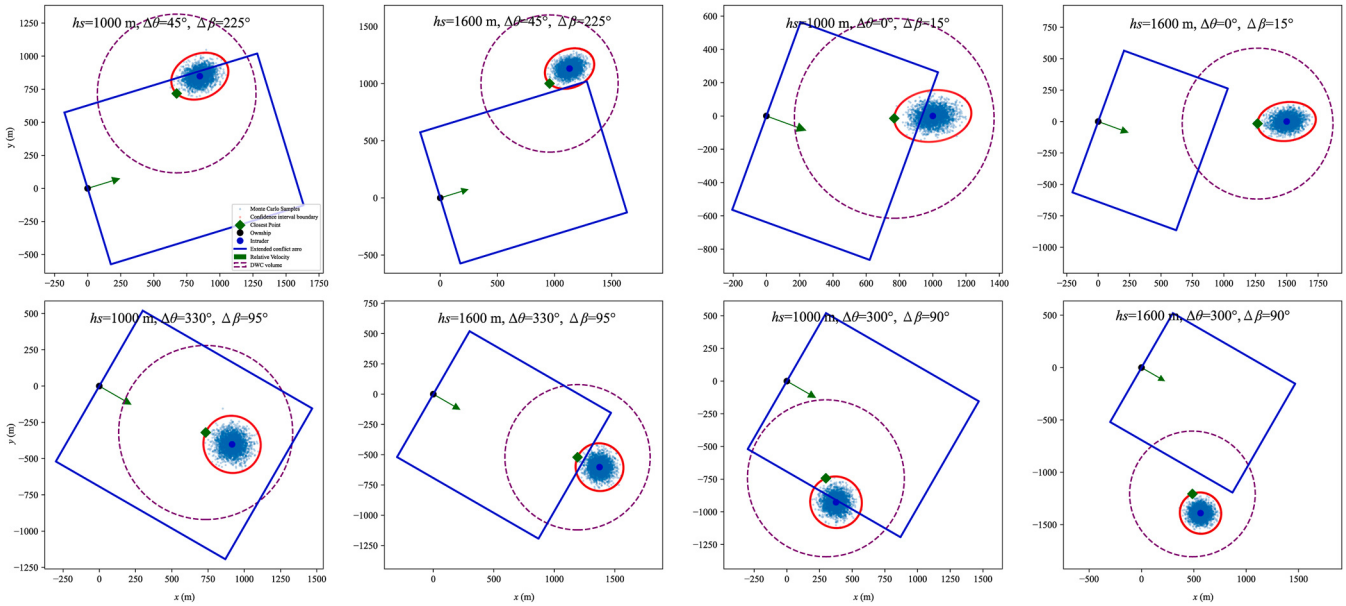


Fig. A1. Graphical explanation of the interactions between strategic mitigation and tactical mitigation.

Fig. A1 illustrates scenarios with typical position–velocity relationships, showing the processes of strategic and tactical mitigation while accounting for their interactions. The blue rectangle represents the extended conflict zone, used to calculate the probability of strategic mitigation failure due to position uncertainty. Blue points indicate the intruder's position distribution under environmental error. Any point falling within the blue rectangle signifies a strategic mitigation failure. Then it is time to tactical mitigation. Under normal circumstances, tactical mitigation is based on the original positions of the two aircraft in the flight plan. However, when accounting for the interactions, that is, considering the positional uncertainty arising in strategic mitigation, a conservative approach is adopted: using the red curve to depict the 95% confidence interval of the intruder's position distribution, encompassing most of the possible positions. The point on the curve closest to the ownship is selected as the intruder's actual position. A dashed circular centered on this position represents the collision envelope, while the green arrow indicates the relative velocity vector between the two aircraft, serving as the starting point for tactical mitigation.

To demonstrate the applicability of the improved model presented above, we added a Monte Carlo simulation that covers the entire phase from strategic mitigation to collision avoidance. Some small-angle encounter scenarios are constructed in the simulation by varying the azimuth, relative velocity, and horizontal distance between two aircraft. The simulation process is similar to that in Sections 4.2 and 4.3. Both the strategic and tactical phases were simulated 10,000 times. During the transition from strategic to tactical mitigation, the actual position of the intruder is selected as the point closest to the ownship among all simulated points.

Table A1
Monte carlo simulation results: computed minus assessed mitigation failure probability based on 10,000 samples per entry.

Azimuth (°)		Heading angle of relative velocity (°)				
		Horizontal separation (m)				
		900	1000	1100	1200	1400
0	0	+0.039	+0.023	+0.018	+0.009	+0.001
0	10	+0.054	+0.022	+0.026	+0.005	+0.002
0	20	+0.068	+0.014	+0.009	+0.004	0.000
30	10	+0.083	+0.011	+0.008	+0.001	0.000
30	20	+0.065	+0.031	+0.026	+0.012	+0.002
30	30	+0.015	+0.044	+0.030	+0.065	+0.005

Table A1 presents the error values, defined as the difference between the simulation results and the assessed results, for various combinations of azimuth, heading angle of relative velocity, and horizontal separation. Positive values indicate that the simulation overestimates the assessment result. In the assessment model, the intruder's position is represented by the point on the confidence curve nearest to the ownship, whereas in the simulation, the intruder's position is taken directly as the closest point among all simulated points. The latter approach is more conservative, which tends to produce relatively higher simulation results. Overall, in scenarios where the ownship and the intruder encounter at small angles and short distances, the maximum error is 0.083. Therefore, the model that accounts for interactions between strategic and tactical measures can still ensure high accuracy.

The method presented in the Appendix can serve as a reference for extending the SWM model, addressing concerns regarding its independence assumption, and providing valuable guidance on how to account for interactions between adjacent layers.

References

ASTM International, 2020. Standard specification for detect and avoid system performance requirements. https://img.antpedia.com/standard/files/pdfs_ora/20230612/astm/2023/F.

Chandler, H.E., Giesecke, W., 1983. Technical writer's handbook. IEEE Trans. Prof. Commun. 2, 90–90.

Choi, M., Rubenecia, A., Shon, T., Choi, H.H., 2017. Velocity obstacle based 3D collision avoidance scheme for low-cost micro UAVs. Sustainability 9, 1174.

Cone, A.C., Wu, M.G., Lee, S.M., 2019. Detect-and-avoid alerting performance for high-speed UAS and non-cooperative aircraft. In: AIAA Aviation 2019 Forum, p. 3313.

Dekker, S., 2017. The Field Guide to Human Error Investigations. Routledge, London, UK.

Federal Aviation Administration, 1988. Pilot windshear guide. https://www.scribd.com/document/466752768/FAA-Pilot-Wind-Shear-Guide-pdf.

Fellner, A., Konieczka, R., 2019. Rotorcraft in the performance based navigation international civil aviation organization implementation. Trans. Aerosp. Res. 254, 53–64.

Garrow, L.A., German, B.J., Leonard, C.E., 2021. Urban air mobility: a comprehensive review and comparative analysis with autonomous and electric ground transportation for informing future research. Transport. Res. C Emerg. Technol. 132, 103377.

Hongsheng, Z., Xiaohao, X., Zhang, J., Yanbo, Z., Chuansen, Y., Sheng, H., 2011. Lateral flight technical error estimation model for performance based navigation. Chin. J. Aeronaut. 24, 329–336.

Hu, X., Pang, B., Dai, F., Low, K.H., 2020. Risk assessment model for UAV cost-effective path planning in urban environments. IEEE Access 8, 150162–150173.

International Civil Aviation Organization (ICAO), 2018. Safety management anual (SMM). https://tools.safran-helicopter-engines.com/document/documentServlet/us/1/8/4618454/ICAO_SMM.PDF.

International Organization for Standardization (ISO), 2023. Flight control system for civil small and light multicopter unmanned aircraft system (UAS) — general requirements. https://cdn.standards.iteh.ai/samples/78483/2741a40aed374be19a96cd48114e9aa1/ISO-24355-2023.pdf.

Joint Authorities for Rulemaking of Unmanned Systems (JARUS), 2024. JARUS guidelines on specific operations risk assessment (SORA). http://jarus-rpas.org/wp-content/uploads/2024/06/SORA-v2.5-Main-Body-Release-JAR_doc_25.pdf.

la Cour-Harbo, A., Schiøler, H., 2019. Probability of low-altitude midair collision between general aviation and unmanned aircraft. Risk Anal. 39, 2499–2513.

Liu, W., Hwang, I., 2011. Probabilistic trajectory prediction and conflict detection for air traffic control. J. Guid. Control Dynam. 34, 1779–1789.

Lum, C., Waggoner, B., 2011. A risk based paradigm and model for unmanned aerial systems in the national airspace. In: Infotech@ Aerospace 2011, p. 1424.

McFadyen, A., Martin, T., Perez, T., 2018. Low-level collision risk modelling for unmanned aircraft integration and management. In: 2018 IEEE Aerospace Conference, pp. 1–10.

Miles, T., Suarez, B., Kunzi, F., Jackson, R., 2019. SORA application to large RPAS flight plans. In: 2019 IEEE/AIAA 38th Digital Avionics Systems Conference (DASC), pp. 1–6.

Muñoz, C., Narkawicz, A., Hagen, G., Upchurch, J., Dutle, A., Consiglio, M., et al., 2015. DAIDALUS: detect and avoid alerting logic for unmanned systems. In: 2015 IEEE/AIAA 34th Digital Avionics Systems Conference (DASC), 5A1–1–5A1–12.

Paielli, R.A., Erzberger, H., 1997. Conflict probability estimation for free flight. J. Guid. Control Dynam. 20, 588–596.

Pang, B., Zhang, M., Deng, C., Low, K.H., 2022. Investigation of flight technical error for UAV separation requirement based on flight trajectory data. In: AIAA Aviation 2022 Forum, p. 3763.

Pothana, P., Joy, J., Snyder, P., Vidhyadharan, S., 2023. Uas air-risk assessment in and around airports. In: 2023 Integrated Communication, Navigation and Surveillance Conference (ICNS), pp. 1–11.

Reason, J., Hollnagel, E., Paries, J., 2006. Revisiting the Swiss cheese model of accidents. J. Clin. Eng. 27, 110–115.

Saeed, F., Mehmood, A., Majeed, M.F., Maple, C., Saeed, K., Khattak, M.K., et al., 2021. Smart delivery and retrieval of swab collection kit for COVID-19 test using autonomous unmanned aerial vehicles. Phys. Commun. 48, 101373.

Schwoch, G., Lieb, T.J., Shamim, M., Vanhandenhove, G., 2024. Interaction between ATM and UAS operators in U-space operations and potential automation benefits. In: 2024 Integrated Communications, Navigation and Surveillance Conference (ICNS), pp. 1–9.

Scott, B.I., Andritsos, K.I., 2023. A drone strategy 2.0 for a smart and sustainable unmanned aircraft eco-system in Europe. Air Space Law 48, 273–296.

Shively, R.J., Vu, K.-P.L., Buker, T.J., 2013. Unmanned aircraft system response to air traffic control clearances: measured response. In: Proceedings of the Human Factors and Ergonomics Society Annual Meeting, pp. 31–35.

Su, Y., Xu, Y., 2024. A risk assessment method for mid-air collisions in urban air mobility operations. IEEE Trans. Intell. Veh. 10, 1327–1341.

Teutsch, J., 2023. Dynamic airspace re-configuration for drones with varying mission requirements: the evolution from project AURA to project ENSURE. https://hdl.handle.net/10921/1720.

Velasco, G.A.M., Borst, C., Ellerbroek, J., Van Paassen, M., Mulder, M., 2015. The use of intent information in conflict detection and resolution models based on dynamic velocity obstacles. IEEE Trans. Intell. Transport. Syst. 16, 2297–2302.

Vila Carbó, J.A., Balbastre Tejedor, J.V., Morcillo Pallarés, P., Yuste Pérez, P., 2023. Risk-based method for determining separation minima in unmanned aircraft systems. J. Air Transport. 31, 57–67.

Wang, C.J., Tan, S.K., Ting, L.K.J., Low, K.H., 2018. Impact of sensors on collision risk prediction for non-cooperative traffic in terminal airspace. In: 2018 International Conference on Unmanned Aircraft Systems (ICUAS), pp. 177–185.

Wang, C.J., Tan, S.K., Low, K.H., 2019. Collision risk management for non-cooperative UAS traffic in airport-restricted airspace with alert zones based on probabilistic conflict map. Transport. Res. C Emerg. Technol. 109, 19–39.

Wang, C.J., Tan, S.K., Low, K.H., 2020. Three-dimensional (3D) Monte-Carlo modeling for UAS collision risk management in restricted airport airspace. Aero. Sci. Technol. 105, 105964.

Wang, C.J., Ng, E.M., Low, K.H., 2021. Investigation and modeling of flight technical error (FTE) associated with UAS operating with and without pilot guidance. IEEE Trans. Veh. Technol. 70, 12389–12401.

Xiang, J., Liu, Y., Luo, Z., 2016. Flight safety measurements of UAVs in congested airspace. Chin. J. Aeronaut. 29, 1355–1366.

Xue, Y., Fu, G., 2018. A modified accident analysis and investigation model for the general aviation industry: emphasizing on human and organizational factors. J. Saf. Res. 67, 1–15.

Zhang, H., Zhang, J., Zhong, G., Liu, H., Liu, W., 2022. Multivariate combined collision detection for multi-unmanned aircraft systems. IEEE Access 10, 103827–103839.

Zhong, G., Du, S., Zhang, H., Zhou, J., Liu, H., 2024. Demarcation method of safety separations for sUAV based on collision risk estimation. Reliab. Eng. Syst. Saf. 242, 109738.

Zou, Y., Zhang, H., Zhong, G., Liu, H., Feng, D., 2021. Collision probability estimation for small unmanned aircraft systems. Reliab. Eng. Syst. Saf. 213, 107619.



Jinpeng Zhang received the M.S. degree in transportation engineering from Nanjing University of Aeronautics and Astronautics, China, in 2024. He is pursuing the Ph.D. degree at Beihang University, China. His research focuses on risk assessment and control for UAS operations in urban air mobility, with particular interests in mid-air collision probability assessment, third-party risk modeling, and risk-aware autonomous interval management for multi-aircraft operations.



Yan Xu is a Professor with the School of Electronic and Information Engineering at Beihang University. Before joining Beihang University, he was a Senior Lecturer in ATM/CNS, with the School of Aerospace, Transport and Manufacturing at Cranfield University. He was the Course Director of the newly established MSc in Advanced Air Mobility Systems, also leading the Air Traffic Management Laboratory based in the Digital Aviation Research and Technology Centre. He conducted postdoc research with the same school as a Research Fellow in UAS Traffic Management. Prior to joining Cranfield University, he received the Ph.D. degree in aerospace science and technology from the Technical University of Catalonia, and received the M.S. and B.S. degrees in traffic engineering from Nanjing University of Aeronautics and Astronautics. He performed a visiting study in early 2017 at the Ecole Nationale de l'Aviation Civile. His main research interests include air traffic management, UAS traffic management, and Urban Air Mobility.



Kaiquan Cai received the B.S. and Ph.D. degrees from Beihang University in 2004 and 2013, respectively. He is currently an Associate Dean and a Professor with the School of Electronic and Information Engineering, Beihang University, and the Deputy Director of State Key Laboratory of CNS/ATM. His research interests include intelligent air navigation and networked collaborative air traffic management.



Victor Gordo holds the M.S. degree in aeronautical engineering and has 25 years of experience in the field of air navigation systems. He specializes in navigation aids, satellite navigation, and surveillance systems, and has managed European GNSS Agency (GSA)-funded projects for E-GNSS implementation. He is currently engaged in UAS operations and U-space development, contributing to SESAR JU projects and providing expert support for EASA's international programs. He is also an active member of standardization and vision groups, including EUROCAE WG-105 (UAS), WG-115 (C-UAS), the U-space Coordination Cell, and the ICAO AAM Study Group.



Gokhan Inalhan is the Executive Director of the Sloane Institute in London and the Chief Technology Officer of Altay Technology Group. He holds the Ph.D. and M.S. degrees in aeronautics and astronautics from Stanford University. He has successfully led numerous large-scale R&D programs funded by the European Commission (FP7, H2020, SESAR, Marie-Curie), UKRI, EPSRC, Innovate UK, and TUBITAK. He has held senior academic roles, including Director General of the Aerospace Research Center at Istanbul Technical University and BAE Systems Chair at Cranfield University. He currently serves as Chair of the *IEEE Technical Committee on Aerospace Control* and Editor-in-Chief of *IEEE Transactions on Aerospace and Electronic Systems*. He is a Fellow of IKE Institute and an Associate Fellow and lifetime member of AIAA.